J Neurophysiol 100: 1770–1799, 2008.
First published July 23, 2008; doi:10.1152/jn.90416.2008.

Reconfiguration of the Pontomedullary Respiratory Network: A Computational Modeling Study With Coordinated In Vivo Experiments

I. A. Rybak,[1] R. O'Connor,[2] A. Ross,[2] N. A. Shevtsova,[1] S. C. Nuding,[2] L. S. Segers,[2] R. Shannon,[2] T. E. Dick,[3] W. L. Dunin-Barkowski,[4,5] J. M. Orem,[5] I. C. Solomon,[6] K. F. Morris,[2] and B. G. Lindsey[2]

[1]*Department of Neurobiology and Anatomy, Drexel University College of Medicine, Philadelphia, Pennsylvania;* [2]*Department of Molecular Pharmacology and Physiology and Neuroscience Program, School of Biomedical Sciences, University of South Florida College of Medicine, Tampa, Florida;* [3]*Departments of Medicine and Neurosciences, Case Western Reserve University, Cleveland, Ohio;* [4]*Department of Neuro-Optical Systems, Scientific-Research Institute for System Analysis, Russian Academy of Sciences, Moscow, Russia;* [5]*Department of Physiology, Texas Tech University Health Sciences Center, Lubbock, Texas; and* [6]*Department of Physiology and Biophysics, State University of New York, Stony Brook, New York*

Submitted 28 March 2008; accepted in final form 16 July 2008

Rybak IA, O'Connor R, Ross A, Shevtsova NA, Nuding SC, Segers LS, Shannon R, Dick TE, Dunin-Barkowski WL, Orem JM, Solomon IC, Morris KF, Lindsey BG. Reconfiguration of the pontomedullary respiratory network: a computational modeling study with coordinated in vivo experiments. *J Neurophysiol* 100: 1770–1799, 2008. First published July 23, 2008; doi:10.1152/jn.90416.2008. A large body of data suggests that the pontine respiratory group (PRG) is involved in respiratory phase-switching and the reconfiguration of the brain stem respiratory network. However, connectivity between the PRG and ventral respiratory column (VRC) in computational models has been largely ad hoc. We developed a network model with PRG-VRC connectivity inferred from coordinated in vivo experiments. Neurons were modeled in the "integrate-and-fire" style; some neurons had pacemaker properties derived from the model of Breen et al. We recapitulated earlier modeling results, including reproduction of activity profiles of different respiratory neurons and motor outputs, and their changes under different conditions (vagotomy, pontine lesions, etc.). The model also reproduced characteristic changes in neuronal and motor patterns observed in vivo during fictive cough and during hypoxia in non-rapid eye movement sleep. Our simulations suggested possible mechanisms for respiratory pattern reorganization during these behaviors. The model predicted that network- and pacemaker-generated rhythms could be co-expressed during the transition from gasping to eupnea, producing a combined "burst-ramp" pattern of phrenic discharges. To test this prediction, phrenic activity and multiple single neuron spike trains were monitored in vagotomized, decerebrate, immobilized, thoracotomized, and artificially ventilated cats during hypoxia and recovery. In most experiments, phrenic discharge patterns during recovery from hypoxia were similar to those predicted by the model. We conclude that under certain conditions, e.g., during recovery from severe brain hypoxia, components of a distributed network activity present during eupnea can be co-expressed with gasp patterns generated by a distinct, functionally "simplified" mechanism.

INTRODUCTION

The respiratory rhythm is generated by interacting populations of neurons distributed within a neuronal column located in the ventrolateral medulla. Neurons within this "ventrolateral respiratory column" (VRC) can be classified by firing activity relative to the respiratory cycle, biophysical properties including ion channels and receptors, synaptic interactions within the column, projections to other brain regions, and responses to numerous physiological challenges (Alheid et al. 2002; Bianchi et al. 1995; Cohen 1979; Duffin 2004; Feldman 1986; Feldman et al. 2003; Lindsey et al. 2000; Richter and Spyer 2001; Segers et al. 2008; von Euler 1986). Contemporary views consider this column to include (in the rostral-to-caudal direction) the retrotrapezoid nucleus (RTN), the Bötzinger (BötC) and pre-Bötzinger (pre-BötC) complexes, and the rostral and caudal ventral respiratory groups (rVRG and cVRG, respectively) (Alheid et al. 2002; Feldman and Del Negro 2006; Onimaru et al. 2006; Rybak et al. 2007a; Smith et al. 1991, 2007). Some of the VRC populations may include neurons with specific biophysical properties defined by different ionic channels, such as persistent sodium (Butera 1999; Del Negro et al. 2002; Pace et al. 2007a; Rybak et al. 2002, 2003a,b, 2004a,b, 2007a; Smith et al. 2007), calcium (Elsen and Ramirez 1998; Pierrefiche et al. 1999), calcium-activated potassium (Richter et al. 1993), and other channels (Pace et al. 2007b; Pierrefiche et al. 2004), which allow these populations to generate endogenous bursting activity under certain conditions. Endogenous oscillations may play a predominant role in rhythm generation during early development (Duffin 2004) and/or when the network reconfigures during physiological state changes, as in the transformation from eupnea to gasping during hypoxia (Paton et al. 2006; Rybak et al. 2002, 2003b, 2007a,b; St-John and Paton 2003a,b; St-John et al. 2002).

The VRC is embedded in a larger network and interacts with other brain stem regions including the nucleus tractus solitarius (NTS) (Bianchi et al. 1995; Kubin et al. 2006), medullary raphé nuclei (Lindsey et al. 1994), and several pontine nuclei collectively termed the pontine respiratory group (PRG) (Alheid et al. 2004; Dick et al. 1994; Ezure and Tanaka 2006; Segers et al. 2008; Wang et al. 1993). The PRG has been proposed to contribute to respiratory phase-switching (Cohen and Shaw 2004; Haji et al. 2002; Okazaki et al. 2002; Rybak et al. 2004a), modulation of the network in responses to changes in physiological conditions (e.g., altered chemical drive or blood pressure) (Felder and Mifflin 1988; Hamilton et al. 1981; Hsieh et al. 2004; Lara et al. 1994; Song and Poon 2004), reconfiguration of the network during sleep states

Address for reprint requests and other correspondence: B. G. Lindsey, Dept. of Molecular Pharmacology and Physiology, School of Biomedical Sciences, College of Medicine, University of South Florida, 12901 Bruce B. Downs Blvd., Tampa, FL 33612 (E-mail: blindsey@health.usf.edu).

The costs of publication of this article were defrayed in part by the payment of page charges. The article must therefore be hereby marked "*advertisement*" in accordance with 18 U.S.C. Section 1734 solely to indicate this fact.

(Douglas et al. 2004; Kubin and Fenik 2004; Radulovacki et al. 2004), entrainment by somatic afferent stimulation (Potts et al. 2005), and other breathing-related behaviors (e.g., coughing) (Shannon et al. 2004a,b).

Several previous computational models of respiratory rhythm generation contributed to our understanding of the respiratory brain stem (e.g., see Balis et al. 1994; Butera et al. 1999; Duffin 1991; Duffin et al. 1995; Dunin-Barkowski et al. 2003; Gottschalk et al. 1994; Lindsey et al. 2000; Ogilvie et al. 1992; Rybak et al. 1997a,b; Smith et al. 2000). These models, however, did not consider spatial compartmentalization of respiratory neuron populations within the VRC, nor did they consider a possible role of the PRG in respiratory rhythm and pattern generation. Rybak et al. (2004a, 2007a) and Smith et al. (2007) made a first attempt to consider in modeling a spatially compartmentalized pontomedullary network. However, in the models by Rybak et al. (2007a) and Smith et al. (2007), the pontine compartment provided drive to VRC but did not contain neural populations, and in the model by Rybak et al. (2004a), connections between PRG and VRC were largely ad hoc and no connections were considered within the PRG. As reported in the preceding companion paper (Segers et al. 2008), we have now identified numerous interactions among PRG neurons and between the VRC and PRG using in vivo multi-array recording technology and spike train analysis.

The present study had three major objectives. The first was to extend current computational models of the pontomedullary respiratory network by incorporating the PRG and functional connections of pontine neurons identified during coordinated experimental studies (Segers et al. 2008). In new models described herein, the respiratory modulation of PRG neurons is due to both inputs from the VRC and connectivity within the PRG. In contrast to a previous model (Balis et al. 1994), the new models incorporate an enhanced "I-Driver" or "I-E/I" pre-BötC population of neurons with conditional pacemaker properties that allow this population to generate intrinsic oscillations under certain conditions (see Rybak et al. 2004a, 2007a; Smith et al. 2007). Starting with an initial model, development was done with the goal of recapitulating all earlier modeling results on alterations in neuronal discharge profiles and motor patterns following removal of vagal pulmonary stretch receptor (PSR) feedback and various pontine lesions (Rybak et al. 2004a).

Our second objective was to simulate and reproduce the specific changes in neuronal discharge profiles and motor patterns observed under different experimental conditions in other coordinated in vivo studies (Lovering et al. 2006; Shannon et al. 2004a,b) and earlier work (Shannon et al. 1998, 2000). Our approach here was to reproduce these changes in the neuronal and motor patterns by altering the excitability of particular neural populations in the model; this allowed us to make specific predictions about potential mechanisms underlying the changes observed in these patterns. Specifically, we considered alterations in neuronal and motor patterns observed during fictive cough, an airway defensive reflex, and moderate hypoxia in non-rapid eye movement (NREM) sleep.

The third objective was to investigate specific relationships between network and pacemaker rhythm-generating mechanisms. Studies of Paton et al. (2006) provided evidence for a hypoxia-driven transformation within the brain stem respiratory network in which gasping relies on intrinsic persistent sodium (I_{NaP})-dependent bursting pacemaker mechanisms, whereas normal breathing (eupnea) does not depend on this cellular mechanism and relies on network interactions within the brain stem respiratory center. Recent experimental and modeling studies (Rybak et al. 2007a; Smith et al. 2007) have also demonstrated the presence of a network and I_{NaP}-dependent pacemaker mechanisms that may be uncovered by brain stem transections so that with reduction of the respiratory network by removing the pons and more rostral medullary compartments, the rhythmogenic mechanism switches from a network-based to a pacemaker-driven I_{NaP}-dependent process. Based on these previous studies, I_{NaP}-based intrinsic bursting properties have been incorporated into our model's I-Driver neurons of pre-BötC. Interestingly, our preliminary simulation results predicted that network-based and pacemaker-driven rhythms can be co-expressed under certain conditions, resulting in a "burst-ramp" motor pattern. We tested the prediction in vivo and demonstrated that such complex motor patterns may indeed occur in certain conditions, for example, during the recovery of respiratory network activity after hypoxia-induced gasping.

Preliminary accounts of this work have been reported (Lindsey et al. 2005, 2007; Morris et al. 2005; Shannon et al. 2006).

METHODS

Simulations

All simulations were performed using an upgraded version of our custom software package that was developed based on the SYSTM11 program by MacGregor (1987; see details in Balis et al. 1994). The upgraded version of the package was implemented using the C language in the UNIX environment. All models presented in this paper describe interacting populations of neurons simulated in the "integrate-and-fire" (IF) style. Although a series of recent models employed neuron models developed in the Hodgkin-Huxley style (e.g., Rybak et al. 2004a, 2007a; Smith et al. 2007), IF models provide a computationally more efficient and appropriate alternative because many of the parameters in the conductance-based models are unknown. Moreover, the (pseudo) activity profiles generated by the IF style models, even though there is no explicit spike generation mechanism, can resemble recorded spiking patterns of the different classes of respiratory neurons incorporated in the model. The detailed formal descriptions of IF neuron models used in our simulations (except those for I-Driver neurons) and their parameters can be found in MacGregor (1987). We explicitly used these neuron models and our simulation package was based on MacGregor's SYSTEM11 program (MacGregor 1987). Slow dynamics of the threshold for spike generation (activity-dependent increase of the threshold) were incorporated in models of neurons with adaptive firing behavior (i.e., neurons responded to a stepwise excitation with an initial increase in the spike frequency followed by a slow reduction of the frequency to a steady state level) (see Balis et al. 1994; MacGregor 1987). To model the I-Driver (I-E/I) population of pre-BötC neurons with conditional I_{NaP}-dependent bursting properties, a simplified description for such neurons in the IF style was derived from the model of Breen et al. (2003) that reproduced I_{NaP}-dependent bursting behavior of the previous pacemaker bursting neuron model developed in the Hodgkin-Huxley style (Butera et al. 1999); parameters are listed in Table A2, APPENDIX. Excitability of each neuron was regulated by synaptic currents, an injected current to the neuron, and noise added to provide variability in the activity of each neuron. External drives to the network were simulated as synaptic inputs from "fiber populations." At each integration step (0.5 ms), the simulator updated state variables for membrane potential (E_{ij}), spike-generation threshold (TH_{ij}), post action potential potassium conductance (GK_{ij}), and synaptic conduc-

tances (G_{ijk}) for each neuron (j) of each population (i) and each synaptic type (k). When the membrane potential of any cell exceeded the cell's threshold for spike generation, an action potential was generated (S_{ij}). Simultaneously, the input conductances were activated and all target cells received (after conduction times) input synaptic currents defined by weights of synaptic connections and type of synapses. A simplified model of lung slowly adapting PSR feedback was also incorporated in the model (see Table A3 of the APPENDIX).

Heterogeneity within classes of respiratory neurons was assumed and some types of neurons described in the literature as distinct were grouped, either for simplicity or because different terminology has been used in different papers for neurons with similar discharge patterns and proposed functions. A glossary and key to abbreviations for the specific neuron populations considered in this study and in the models described are summarized in Table 1.

The full model description and model parameters can be found in the APPENDIX. All parameters for the initial model are presented in Tables A1–A4 of the APPENDIX; Tables A5–A8 give extended model parameters. The number of neurons in a population ranged from 99 to 300 (see Tables A1 and A5). The VRC IE population had 99 neurons because cells with this particular discharge pattern were encountered in previous studies less often than other categories of respiratory neurons. Otherwise, no attempt was made to match the relative numbers of different "types" of neurons found in vivo with the numbers of neurons in simulated populations.

Simulations were run on 64-bit Intel and AMD multiprocessor-based computers under the Linux operating system.

In vivo experiments

As detailed subsequently in RESULTS, some connections among neural populations in the initial model were assigned from previously published experimental data, and some were assigned as necessary to provide network mechanisms for rhythm generation. Most connections incorporated in the final extended model were based on the results of coordinated complementary in vivo experiments undertaken and used iteratively to develop and test model-based hypotheses. As described in a companion paper, multiple arrays of microelectrodes with individual depth adjustment were used for extracellular neuronal recordings from the brain stem in vivo and various computational methods were applied to screen the resultant large datasets of simultaneously recorded spike trains (Segers et al. 2008). Extended correlation linkage maps among PRG and VRC neurons were developed and used to screen for the presence of functional connections postulated in our initial model and to guide both the pruning and addition of connections in subsequent revisions of the model.

In the experiments devoted to the study of respiratory neuron activities during hypoxic gasping and recovery reported herein, the general methods were the same as in the companion paper (Segers et al. 2008). All experiments were performed under protocols approved by the University of South Florida's Animal Care and Use

TABLE 1. *Glossary and key to abbreviations for neuronal populations*

Neuronal Population	Description
I-Driver (I-EI)	Excitatory inspiratory neurons in the pre-BotC region that excite other I neurons. During eupnea, they are usually activated before the expiratory-inspiratory phase transition. In our models these neurons have intrinsic, persistent sodium current-dependent pacemaker bursting properties which may be released under certain conditions.
I-Aug (BS)	Inspiratory neurons with an augmenting firing pattern during the inspiratory phase. BS – a subset of bulbospinal I-Aug neurons with axonal projections to spinal cord; does not exclude collateral axons in the brain stem.
I-Dec	Inhibitory inspiratory neurons with a decrementing firing pattern.
ILM	Inspiratory laryngeal motoneuron
IE	Neurons with average peak of firing rate at the inspiratory-to-expiratory (I-to-E) phase transition or at the end of inspiration ("late I").
EI	Neurons with average peak of firing rate at the expiratory-to-inspiratory (E-to-I) phase transition.
E-Aug (-early, -late, -BS, -HT)	Expiratory neurons with an augmenting discharge pattern. "Early" − onset of activity begins early in the phase and continues throughout the phase; includes E-"constant" firing rate pattern (Ezure 1990). "Late" − activity onset is delayed and may be limited primarily to the later half of the expiratory interval (stage 2 expiration). BS − bulbospinal. High-threshold (HT) neurons are a subset of the E-Aug-late population with activity evoked by cough and chemoreceptors.
ELM	Expiratory laryngeal motoneuron
E-Other	Additional expiratory pontine population in initial model
E-Dec (-T, -P)	Expiratory neurons with a decrementing firing rate; most active during the early-expiratory (post-inspiratory) interval: -T and -P represent such populations with tonic and phasic discharge pattern, respectively
NRM (+, −)	Neurons with non-respiratory-modulated activity as judged by statistical methods; (excitatory or inhibitory, respectively).
PRG I	Pontine neuron with a peak firing rate during the second half of the inspiratory phase and with a generally augmenting activity profile during the phase.
PRG E	Pontine neuron with a peak firing rate during the second half of the expiratory phase and with an augmenting activity profile during the phase.
PRG IE	Pontine neuron with a peak firing rate during the I-to-E phase transition and with a decrementing activity profile in the latter phase.
PRG EI	Pontine neuron with a peak firing rate during the E-to-I phase transition and with a decrementing activity profile in the latter phase.
Pump+ and Pump−	Neurons located in the NTS that are excited by pulmonary stretch receptors during lung inflation; do not receive direct central respiratory drive. Pump+ neurons are excitatory; Pump− neurons are inhibitory.
Phrenic (Phr)	Phrenic motoneuron
Lum (Exp MN)	Spinal (Lumbar) motoneurons controlling expiratory muscle.
PSR	Slowly adapting pulmonary stretch receptors
Second order (cough)	Second-order NTS neurons that affect respiratory neurons in both VRC and PRG, causing reconfiguration of the respiratory network to produce the cough motor pattern

Heterogeneity within classes of respiratory neurons was considered and some "types" of neurons described in the literature were grouped together, either for simplicity or because different terminology has been used for neurons with similar discharge patterns and proposed functions as noted elsewhere (e.g., Ezure 1990).

Committee. Animals were initially anesthetized with either intravenous sodium thiopental (22.0 mg/kg) or isoflurane (2–5%) and later decerebrated at the mid-collicular level (Kirsten and St-John 1978). Prior to decerebration, the level of anesthesia was assessed periodically by a noxious stimulus (toe pinch). If the withdrawal reflex occurred or there was an increase in blood pressure or respiration, additional anesthesia was given until the response was absent. Hypoxic gasping was induced by ventilating animals on a gas mixture of 5% O_2-95% N_2. Two statistical tests were performed to evaluate a neuron's respiratory modulation (Morris et al. 1996); firing rate, respiratory cycle-triggered histograms, and a measure of respiratory modulation (Orem and Dick 1983) were calculated for each neuron.

RESULTS

Initial model of the respiratory network: Rationale for initial PRG-VRC network architecture

Our initial model (Fig. 1) incorporated elements of previous large-scale population-based models of the respiratory network (Balis et al. 1994; Lindsey et al. 2000) and, similar to recent models of Rybak et al. (2004a, 2007a) and Smith et al. (2007), explicitly considered the spatial (compartmental) organization of the respiratory network within the brain stem. The following VRC compartments were incorporated in the model (Fig. 1): ventral respiratory group (VRG), pre-BötC, and BötC. The medullary part of the network also included the nucleus of the solitary tract (NTS). The following neural populations were included in the VRC compartments: bulbospinal (BS) I-Aug, IE-VRG, and E-Aug-BS (all in VRG); I-Driver and I-Dec (both in pre-BötC); E-Aug-early, E-Aug-late, E-Dec-P (phasic), E-Dec-T (tonic), and NRM (all in the BötC). The E-Dec-P and E-Dec-T populations have been assumed to have similar inputs. The VRC IE population represents neurons designated by other authors as late-I or Early E-Dec. I-Aug and I-Aug-BS populations were combined into a single population for computational efficiency. The I-Aug population drives the phrenic motoneurons controlling the diaphragm and the E-Aug-BS population drives a population of expiratory motoneurons.

In the initial model, the dorsolateral pons was conditionally subdivided into rostral (rPons) and caudal (cPons) parts (see Fig. 1). Neural populations with inspiratory (I), phase-spanning (rIE) and expiratory (E) modulation were included in the rPons to represent such populations found in the parabrachialis and Kölliker-Fuse nuclei (Alheid et al. 2004; Cohen and Shaw 2004; Dick et al. 1994; Ezure and Tanaka 2006). In keeping with the prior model by Rybak et al. (2004a), the caudal region contained a tonic NRM population to provide an additional pontine drive to the VRC. Based on early preliminary data from the companion study (Segers et al. 2008), a subset of the IE population (cIE), the EI population, and some E neurons were also represented in the caudal region. Table 1 contains explanations of the abbreviations for the neuronal populations considered in this study. Parameters for each population are given in Table A1 of the APPENDIX.

Simplified models of the lungs and slowly adapting PSRs were included in the model and provided pulmonary volume feedback to the respiratory network. This volume feedback operated via the excitatory (Pump+) and inhibitory (Pump−) pump cell populations of NTS. All feedback parameters are given in Table A3 of the APPENDIX.

Connections among neural populations within the VRC (Fig. 1) were assigned based on results from dual neuronal recordings, including both extracellular spike train cross-correlation data and spike-triggered averages of synaptic potentials, published prior to the present study (Anders et al. 1991; Bianchi et al. 1995; Ezure 1990; Feldman and Speck 1983; Jiang and Lipski 1990; Li et al. 1999; Lindsey et al. 1987, 1989a,b, 1998; Morris et al. 1996; Rekling et al. 2000; Segers et al. 1987; Shannon et al. 1998, 2000) or were accepted from previous models (Balis et al. 1994; Lindsey et al. 2000; Rybak et al. 1997a,b, 2004a). Parameters for connections between populations are given in Table A4 of the APPENDIX. Some connections, especially connections between the VRC and the PRG, were assigned ad hoc as necessary to reproduce simulated behaviors.

Interactions within the PRG (among different respiratory-modulated pontine populations) had not been investigated prior to our study described in the companion paper (Segers et al. 2008), and only a few studies have previously addressed the possible interactions between VRC and PRG populations (e.g., Ezure 2004; Segers et al. 1985). In the initial model, some interconnections between the VRC and PRG were based on the early study from our laboratory (Segers et al. 1985) (see green squares in Fig. 1). Other such connections and connections within PRG were incorporated based on general assumptions (yellow triangles). Specifically, we suggested that (see also Segers et al. 2008): *1*) the respiratory modulation of PRG neurons is provided, at least in part, by paucisynaptic inputs from the corresponding VRC populations; *2*) functional connections among PRG neurons contribute to the shaping of their respiratory-modulated activities; *3*) PRG populations project to the VRC populations involved in respiratory phase-switching; and *4*) pericolumnar VRC NRM neurons and pontine NRM neurons have widely distributed functional interactions with respiratory-modulated neurons and modulate their activities.

A few previously identified or postulated neuronal interconnections were also included in the model. Specifically within the rPons, I and E neurons inhibited rIE neurons; within the cPons, E-Other neurons and EI neurons inhibited cIE neurons, whereas NRM cells excited cIE neurons; between the rPons and cPons, E neurons inhibited cPons NRM neurons, and similarly, I neurons inhibited E-Other neurons (see Fig. 1).

The following connections from VRC to rPons populations have been included in the initial model (Fig. 1): *1*) excitatory to I population from I-Aug and inhibitory to this population from E-Dec-P; *2*) excitatory to rIE population from both I-Aug and E-Dec-T, and (iii) excitatory to E population from E-Aug-late. These interactions, together with the hypothesized intrapontine connections, provide I, IE, and E modulation of the corresponding rPons populations (I, rIE and E, respectively). Similarly, the EI population of cPons receives excitation from the medullary I-Dec population. On the other hand, the I population of rPons provides excitation to the medullary I-Aug and IE-VRG populations, the rIE population of rPons excites both E-Dec-P and IE-VRG medullary populations, and the E population of rPons inhibits the I-Dec population. In addition, the cIE population of cPons provides excitation to I-Driver, the EI population of cPons excites both E-Dec-T and IE-VRG, and the NRM population of cPons provides excitatory drive to all medullary respiratory populations except for I-Dec and E-Aug-BS. The model, therefore suggests the existence of spatially organized mutual interactions between VRC populations and several pontine populations (see also Ezure 2004; Gaytán et al. 1997; Núñez-Abades et al. 1993).

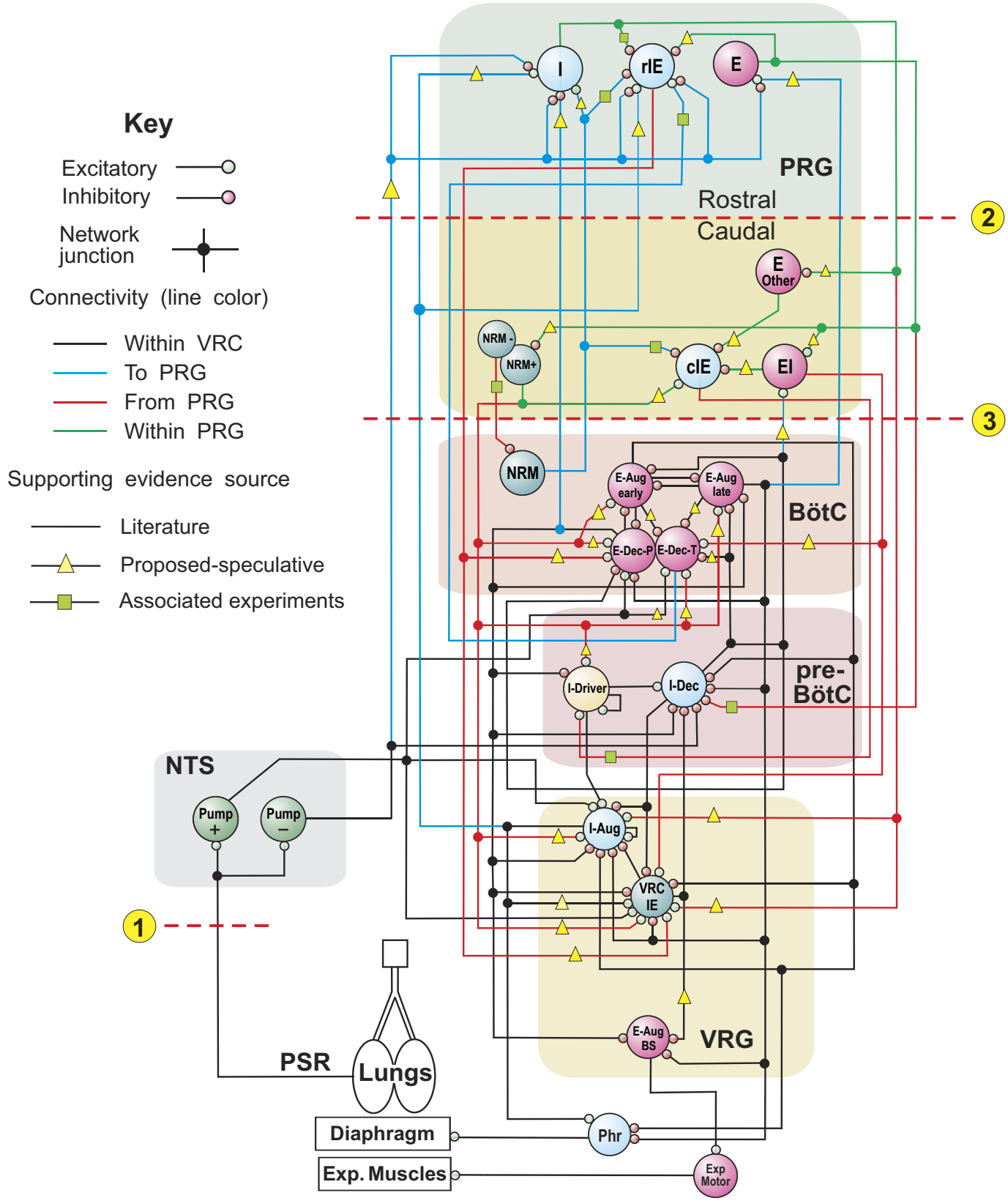

FIG. 1. Schematic of the initial model of the brain stem respiratory network. To facilitate the tracing of pathways, regional connections are color-coded and dots are used to mark branch points of divergent projections. Both evidence-based (see text) and more speculative functional connections are represented in the model (see key). Model parameters for cell properties and connections are detailed in Tables A1–A4 of the APPENDIX. Circled numbers and dashed lines in this and subsequent model diagrams label specific simulated perturbations applied. See text for details.

The PSR afferents activate Pump cells of the NTS, which in turn project to both VRC and PRG (Fig. 1). The Pump cell connections to VRC populations are based in part on previously published in vivo data (Ezure and Tanaka 2004; Kubin et al. 2006); other connections in these particular pathways remain speculative, as do projections of Pump cells to pontine populations that provide presynaptic inhibition of VRC inputs to the PRG as suggested previously (Cohen and Shaw 2004; Feldman et al. 1976; Kubin et al. 2006).

The mean values for weights of all connections were adjusted in the simulations in an attempt to reproduce specific patterns of neural activity observed experimentally or described in the literature.

Performance of the initial model

Network interactions within the VRC among I-Aug, I-Dec, IE and both E-Dec populations (see Fig. 1) define the basic circuitry for the inspiratory off-switch (IOS) mechanism in this model. According to this mechanism, the IE-VRG population (of late-I type) plays a key role in the IOS initiation (Cohen 1979; Cohen and Shaw 2004; Cohen et al. 1993; Haji et al. 2002; Okazaki et al. 2002; Richter 1996; Richter et al. 1986; Rybak et al. 1997a,b, 2004a) by providing initial inhibition of the I-Dec population, resulting in disinhibition of both E-Dec populations, which in turn provide inhibition of all VRC inspiratory populations, thereby completing the transition to expiration. The pontine inputs to the medullary IE-VRG (and, indirectly, to I-Aug and E-Dec-P) population contribute to the IOS mechanism by controlling the transition from inspiration to expiration; hence, these pontine inputs in the model control the duration of inspiration.

Interactions between the E-Dec populations of BötC and the I-Driver population of pre-BötC (see Fig. 1) define the basic circuitry for the expiratory off-switch (EOS) mechanism. During expiration, the I-Driver population is inhibited by both E-Dec populations. As the I-Driver population is released from inhibition and becomes active, it provides initial activation to the I-Dec and I-Aug populations. The I-Dec population inhibits all VRC expiratory populations and hence completes the switch to inspiration. Pontine inputs to the medullary expiratory neurons and I-Driver population contribute to the EOS mechanism controlling the transition from expiration to inspiration; these inputs control the duration of expiration.

Under normal conditions, the initial model generates a stable "eupneic" respiratory rhythm and exhibits realistic firing patterns of individual respiratory neurons (see Fig. 2*A*). Specifically, the firing bursts of individual I-Aug neurons as well as the phrenic discharge exhibit "augmenting" patterns (Fig. 2*A*). The mechanical feedback from PSRs, via the excitatory (Pump+) and inhibitory (Pump−) pump neurons of the NTS, also affect the activity of key neural populations involved in the IOS and EOS mechanisms. Specifically, the excitatory inputs from Pump+ neurons to I-Aug and IE-VRG neurons and the inhibitory input from Pump− cells to I-Dec neurons provide pulmonary feedback control of the IOS mechanism [the inspiration-inhibitory Hering-Breuer (HB) reflex that shortens inspiration; see Fig. 1]. In turn, the excitatory inputs from Pump+ neurons to both E-Dec populations provide the expiration-facilitatory part of the HB reflex. At the same time, the Pump− population, activated by pulmonary feedback, presynaptically inhibits all medullary inputs to rPons (I, rIE, and E populations), thereby suppressing both the respiration-related activities of rPons populations and the pontine control of respiratory phase transitions and phase durations. Importantly, the IOS and EOS mechanisms operate in the model under control of both pontine input and pulmonary feedback (see Cohen and Shaw 2004; Haji et al. 2002; Okazaki et al. 2002; Rybak et al. 2004a). However, with the pulmonary feedback intact, the pontine control of the respiratory motor pattern is suppressed.

Altered patterns with perturbations

Disconnection of PSR feedback in the model increases the amplitude and duration of phrenic discharges (Fig. 2*B;* perturbation 1), reflecting the loss of the HB reflex (e.g., see Bonham and McCrimmon 1990; Clark and von Euler 1972; Cohen 1979; Feldman 1986; Sant'Ambrogio and Widdicombe 2001; von Euler 1986). Also, removal of pulmonary feedback eliminates the suppressing influence of vagal afferents via the Pump− cells of NTS on the pontine (rPons) I, rIE and E populations (see Fig. 1), thereby increasing the role of these populations in the control of respiratory phase switching. This pontine control is provided via the same medullary IOS and EOS circuits that are controlled by pulmonary feedback when the latter are intact (see Cohen and Shaw 2004; Okazaki et al. 2002; Rybak et al. 2004a).

Early studies performed in cats demonstrated that removal of the rostral pons in a vagotomized animal converts eupnea to apneusis, an abnormal breathing pattern that is characterized by a dramatically increased inspiratory duration (Cohen 1979; Marckwald 1887; St-John 1998; Wang et al. 1993). A subsequent complete removal of the pons produces a gasping-like pattern, which therefore may be generated by some mechanisms inherent to the medulla (Lumsden 1923; St-John 1998). Similarly, the removal of rPons in our model converted the eupneic pattern to "apneusis" (Fig. 2*C;* perturbation 2), and the complete elimination of the pons (additional removal of cPons) replaced apneusis with a "gasping-like" pattern (Fig. 2*D*; perturbation 3). The loss of the pons reduced excitatory input to the medullary expiratory neurons (specifically to E-Dec-P and E-Dec-T), resulting in a reduction of the phasic inhibitory influence of E-Dec neurons on the I-Driver population of the pre-BötC (see Fig. 1). In addition, removal of the pons reduced excitatory drive to the medulla, and specifically eliminated tonic drive from the pontine NRM population to I-Driver neurons (see Fig. 1). Both of these factors create the necessary conditions for a release of I_{NaP}-dependent pacemaker-driven activity in the I-Driver population of pre-BötC (see Butera et al. 1999; Rybak et al. 2003b, 2004a,b, 2007a; Smith et al. 2007). The intrinsic I_{NaP}-dependent oscillations of this population now drive the activity in the medullary network and produce output phrenic discharges with a gasping-like (or in vitro-like) shape (see Fig. 2*D*).

In summary, our initial model supports the concept that under normal conditions in vivo, the eupneic respiratory rhythm is generated by network (mostly inhibitory) interactions without involvement of endogenous bursting mechanisms in pre-BötC (in the I-Driver population) that are normally suppressed during eupnea by the pontomedullary interactions (Paton et al. 2006; Rybak et al. 2002; 2004a, 2007a; Smith et al. 2007). During eupnea, the I-Driver population operates in

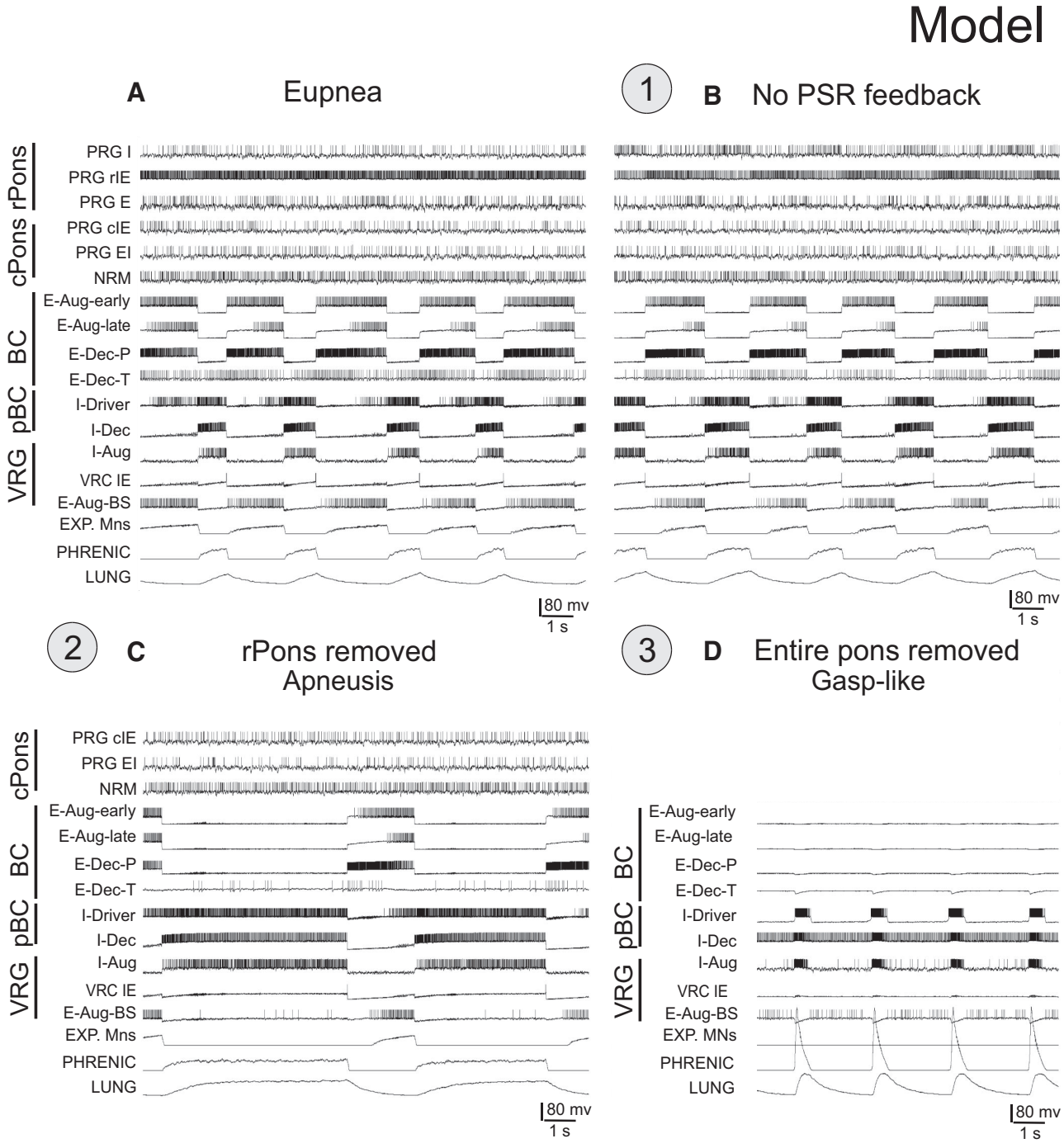

FIG. 2. *A* and *B*: discharge patterns of individual respiratory neurons from each simulated population and network region (labels on the left) and the integrated population traces for expiratory and phrenic motoneurons and lung volume receptors (*3 bottom traces*) during "eupneic" respiratory rhythm (*A*) and following disconnection of lung volume or slowly adapting PSR feedback (*B,*"vagotomy"—perturbation 1—circled here and in Fig. 1), which produced an increase in the amplitude and duration of phrenic discharge. *C*: the effect of rostral pons "removal" (inactivation of populations representing the rostral pons; perturbation 2—circled here and in Fig. 1) resulted in an apneustic pattern with prolonged and irregular inspiratory phase durations. *D*: complete removal of the pons (perturbation 3—circled here and in Fig. 1) led to a gasping-like pattern. See text for details.

a tonic firing state and is inhibited during expiration by expiratory neurons. However, regardless of the operational "state" of the I-Driver population of the pre-BötC, it is a necessary part of the respiratory network. Hence suppression of its activity as illustrated in Fig. 3*A* (perturbation 4), where the I-Driver population was turned off, should normally stop the respiratory pattern. The result is a termination of both network oscillations and output phrenic activity (Fig. 3*B*). At the same time, our simulation demonstrated that a subsequent application of an external tonic excitation of the I-Aug and I-Dec populations (Fig. 3*A,* perturbation 5) can re-establish network oscillations and a normal rhythmic phrenic output (Fig. 3*B*). This property

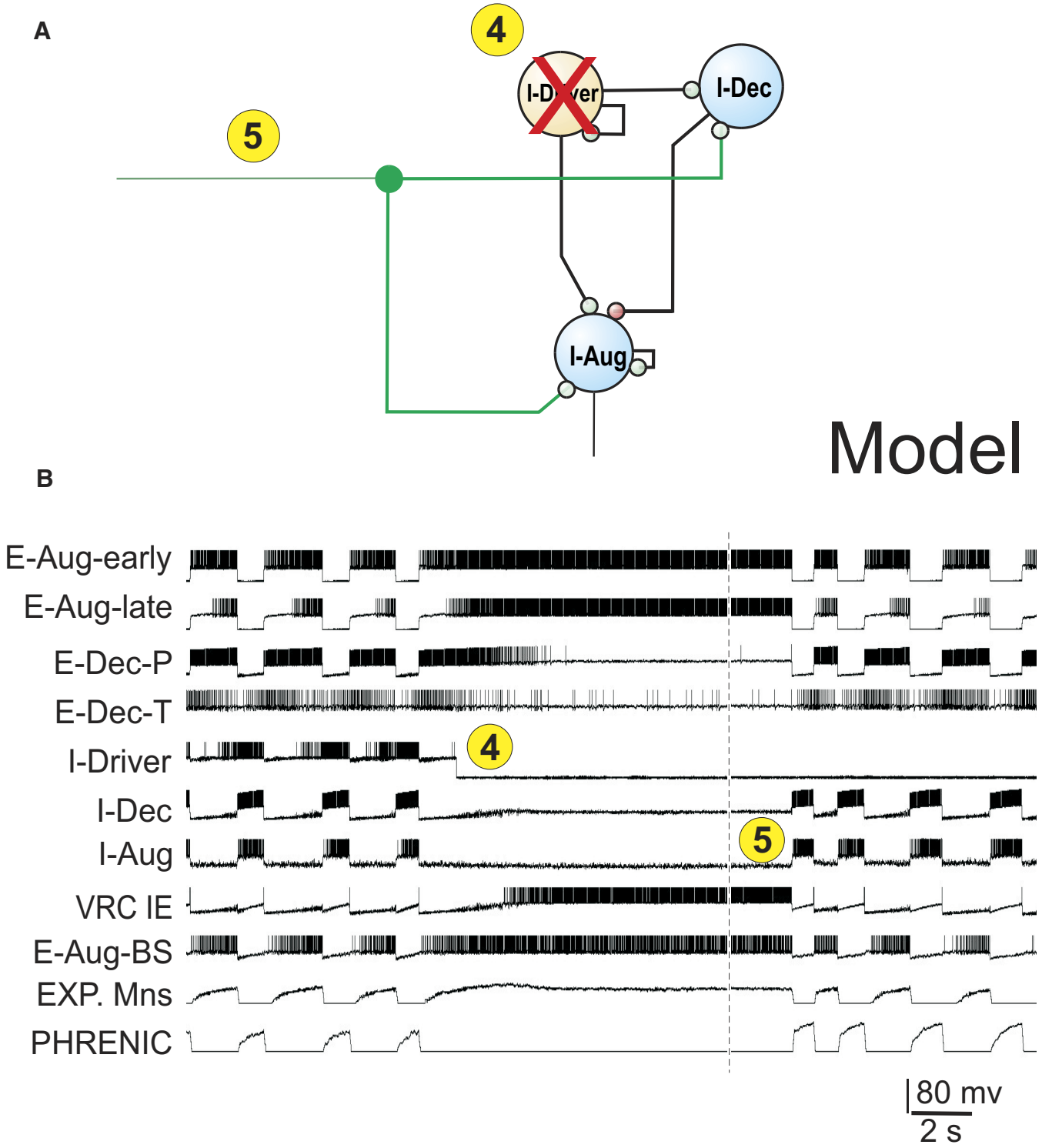

FIG. 3. *A*: schematic of network module illustrating inactivation of the I-Driver population by inhibition (perturbation 4—circled) and subsequent application of external excitatory drive to both I-Aug and I-Dec populations (perturbation 5—circled). *B*: elimination of I-Driver activity terminated both network oscillations and phrenic activity. Subsequent increased excitation of the I-Aug and I-Dec populations (an additional excitatory drive to these populations) re-established network oscillations and a normal rhythmic phrenic output. Vertical dashed line indicates truncation of period without rhythm.

confirmed and extended an earlier modeling result (Balis et al. 1994) which predicted that, under certain conditions, a respiratory rhythm could be generated without the I-Driver population of the pre-BötC. Some implications of this hypothesis are considered later in RESULTS.

Extended model of the brain stem respiratory network

The extended model of the brain stem respiratory network (see schematic in Fig. 4) was developed using the initial model as a basis but incorporated new in vivo data presented in the

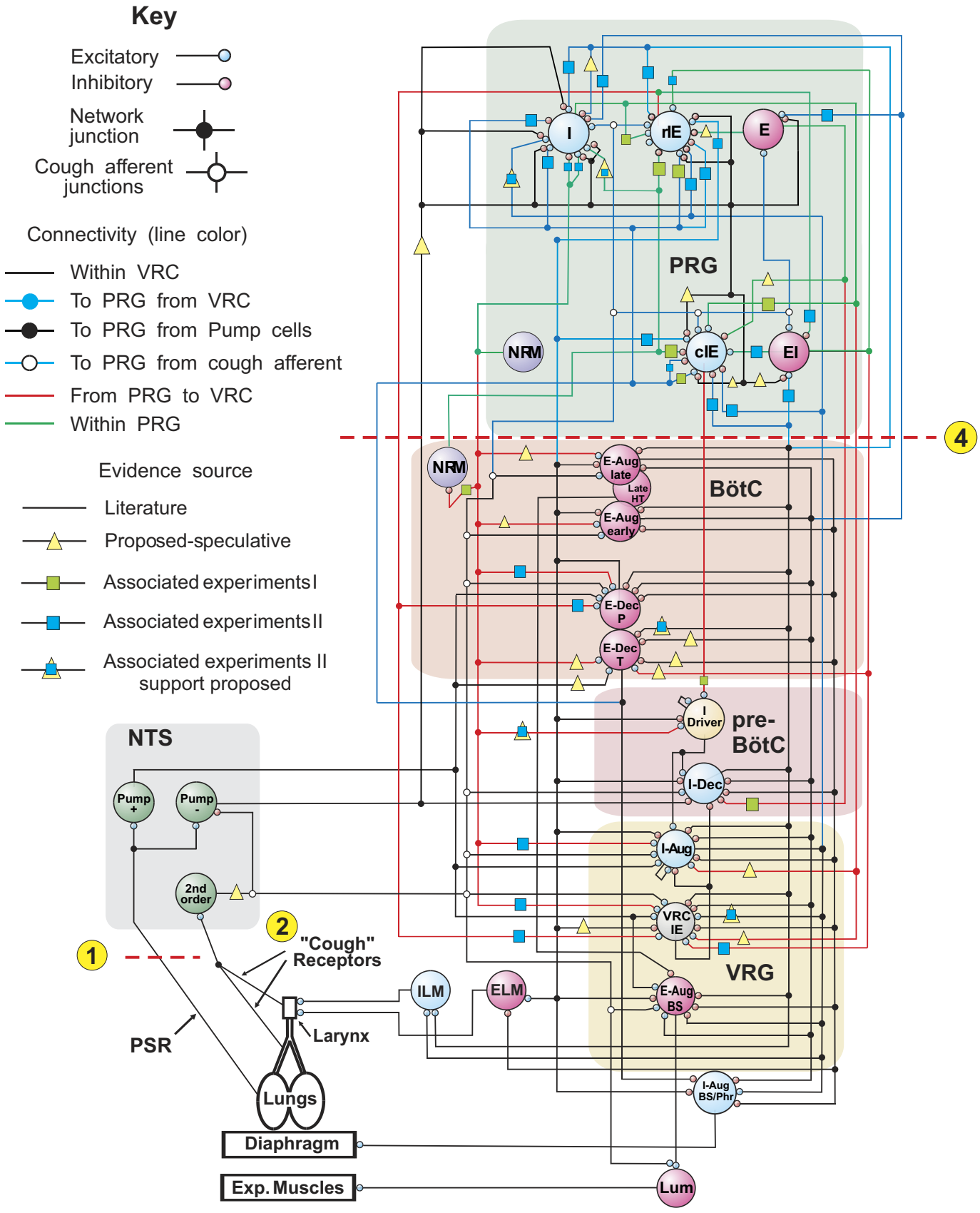
Key
Excitatory
Inhibitory
Network junction
Cough afferent junctions
Connectivity (line color)
Within VRC
To PRG from VRC
To PRG from Pump cells
To PRG from cough afferent
From PRG to VRC
Within PRG
Evidence source
Literature
Proposed-speculative
Associated experiments I
Associated experiments II
Associated experiments II support proposed
I
rIE
E
PRG
NRM
cIE
EI
4
NRM
E-Aug late
Late HT
E-Aug early
BötC
E-Dec P
E-Dec T
I Driver
pre-BötC
I-Dec
I-Aug
VRC IE
VRG
E-Aug BS
I-Aug BS/Phr
NTS
Pump +
Pump -
2nd order
1
2
"Cough" Receptors
ILM
ELM
Larynx
PSR
Lungs
Diaphragm
Exp. Muscles
Lum

companion paper (Segers et al. 2008). The correlation linkage maps described in that paper were used for assigning additional connections in the extended model. The new in vivo data provided experimental support for some connections proposed by the initial model and for many other connections not considered previously, indicating a richer set of functional relationships than initially considered. Note, however, that neurons recorded experimentally were grouped in populations defined primarily by similar discharge patterns in vivo, while the "real" functional neural populations, despite exhibiting similar activity patterns, could have different sources of inputs, provide different actions (excitation and inhibition), and project to different targets.

Overall, the in vivo results supported the four major assumptions that had been used in the initial model as a basis for assigning connections between VRC and PRG populations and within the PRG (see preceding text). Specifically, we initially assumed that *the respiratory modulation of PRG neurons is provided, at least in part, by paucisynaptic inputs from the corresponding VRC populations*, and our in vivo data partly confirmed this assumption. We found a variety of short-time scale correlations between PRG and VRC activities. For example, we found the following functional relationships: VRC I-Aug neurons excite PRG I neurons, both E-Dec-T and E-Dec-P neurons excite PRG IE neurons, and VRC E-Aug neurons excite PRG E neurons and inhibit PRG I neurons. Other detected correlations suggest that VRC I-Dec neurons excite PRG EI and I neurons and inhibit PRG IE neurons.

We also assumed that *functional connections among PRG neurons contribute to the shaping of their respiratory modulated activities*. We did find evidence that, for example, PRG I neurons excite PRG IE neurons, and PRG IE neurons inhibit PRG EI neurons.

Another initial assumption was that *PRG populations project to VRC populations involved in respiratory phase switching*. In support, our in vivo data suggested that PRG IE neurons excite VRC putative I-Driver, VRC IE, and E-Dec neurons. These detected functional connections may explicitly contribute to pontine control of respiratory phase switching.

Finally, we assumed that *pericolumnar VRC NRM neurons and PRG NRM neurons have widely distributed functional interactions with respiratory-modulated neurons.* Evidence from the in vivo experiments supported this assumption. We found, for example, that VRC NRM neurons excite PRG I neurons and inhibit PRG IE neurons; PRG NRM neurons excite PRG I neurons and VRC I-Driver, IE, I-Aug, E-Dec-P, and NRM populations; and PRG NRM neurons inhibit PRG I neurons.

The specific connections mentioned in the preceding text have been incorporated in the extended model (see Fig. 4). In addition, the extended model includes some speculative connections; e.g., those suggested previously in the literature, such as Pump-cell-mediated inhibition in the pons, or those hypothesized during development of the new model as potentially contributing to the shaping of target neuron discharge patterns: PRG I neurons excite VRC I-Aug and IE populations; PRG EI neurons excite VRG E-Dec-T neurons; PRG NRM neurons excite VRC E-Aug-early, E-Aug-late, and E-Dec-T neurons; the VRC I-Dec population inhibits the PRG I population; and PRG E neurons inhibit PRG IE neurons. The IE population was divided into rostral (r) and caudal (c) subsets, with the caudal group (cIE) distinguished by an excitatory input to the I-Driver population as suggested in the companion study (Segers et al. 2008); the majority of IE neurons were recorded in the caudal region of the dorsolateral pontine domain sampled.

Our data suggest that neuronal inputs from the PRG to VRC populations provide a basis for pontine control of phase switching and the durations of inspiratory and expiratory phases. Functional implications of specific connections included in the extended model are considered in subsequent sections of RESULTS. To simulate specific motor behaviors during network reconfigurations, additional connections to premotor (I-Aug-BS and E-Aug-BS) and motoneuron populations, including the inspiratory (ILM) and expiratory (ELM) laryngeal motoneurons, were also added to the extended model. These circuit elements were based on previously reported neuron responses, spike-triggered averages of synaptic potentials or multi-unit nerve recordings, and related circuit models (Baekey et al. 2001, 2004; Ezure 1990; Ezure et al. 1989; Lindsey et al. 1998).

In the course of extended model development, some speculative connections present in the initial model were deleted because of a lack of experimental support or because alternative circuit elements with corresponding functions were implemented (compare the initial model in Fig. 1 with the extended model in Fig. 4 and Table A4 with Table A6 of the APPENDIX). These "pruned" connections included the VRC E-Dec-P neuron inhibition of PRG I neurons (replaced by E-Dec-T inhibition); the VRC E-Aug-late neuron excitation of PRG E neurons (replaced by VRC E-Aug-early excitation); and the PRG E excitation of PRG EI neurons, PRG NRM excitation of PRG cIE neurons, VRC IE inhibition of E-Aug-BS, and the PRG E-Other population and its connections.

Simulations with the extended model

The extended model was able to reproduce all "control" modes of behavior previously demonstrated with the initial model (Fig. 2, *A–D*). For example, Fig. 5 shows a simulation of vagotomy (disconnection of vagal/PSR feedback; perturbation 1). Similar to the initial model, removal of slowly adapting PSR feedback (indicated by the vertical dashed line) produces an increase in the amplitude and duration of phrenic discharges (Fig. 5). In addition, the extended model was able to realistically reproduce and propose plausible network mechanisms for other behaviors as described in the following sections.

Modeling changes of the respiratory motor pattern during cough

The cough reflex is an important airway defensive mechanism. A previous network model and simulations predicted

FIG. 4. Extended model of the pontomedullary respiratory network incorporating connections inferred from results of coordinated in vivo experiments (Segers et al. 2008). Model parameters are detailed in Tables A5 and A6 of the APPENDIX. A subset of the E-Aug-late population had a higher threshold and was designated E-Aug-late-HT. Same labeling conventions as in Fig. 1; key indicates speculative connections that were proposed in the initial model and confirmed (yellow triangles overlaid with blue squares), connections carried over from the initial model that were based on preliminary results of the work presented in Segers et al. (2008), and "new" connections suggested by later results in the study of Segers et al. (2008). See text for details.

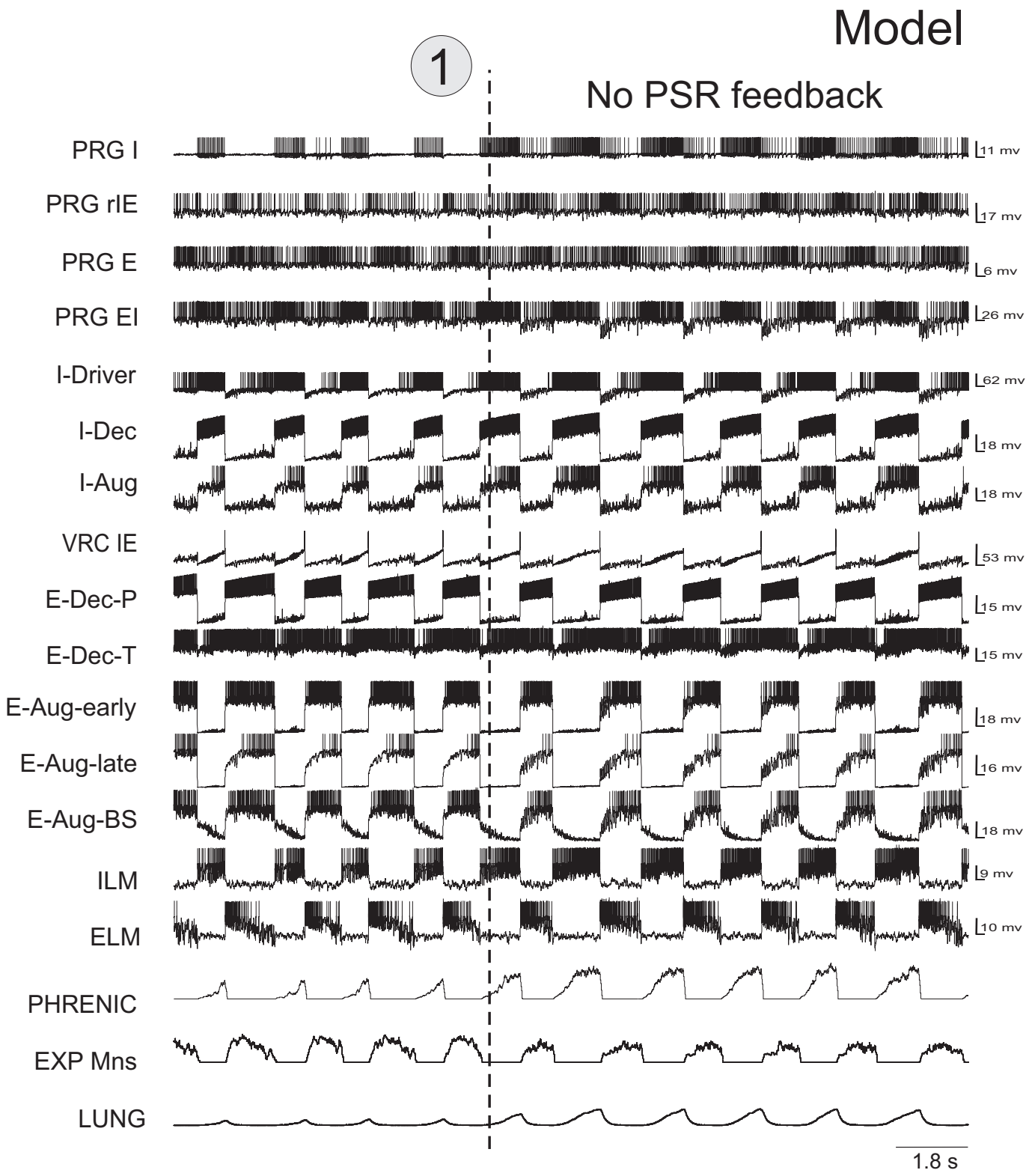

FIG. 5. Removal of slowly adapting PSR feedback in the extended model (perturbation 1 "vagotomy"; vertical dashed line) produced an increase in the amplitude and duration of phrenic discharges.

important roles for, and the reconfiguration of, the ventrolateral medullary respiratory network during cough (Shannon et al. 1998). Subsequent parallel neuron recordings in vivo and correlation analysis supported many of the model's predictions and suggested specific network interactions involved in cough motor pattern generation (Shannon et al. 2000).

Our extended model incorporated earlier hypotheses and proposed that activation of airway cough receptors changes

firing activity of second-order NTS neurons that affect (directly or indirectly) different respiratory neurons in both VRC and PRG, causing reconfiguration of the respiratory network to produce the cough motor pattern—acting, at least in part, through the same VRC neurons involved in providing drive to muscles during normal breathing. To simulate the motor pattern reorganization during cough, all VRC populations (except I-Driver and E-Dec-T) were excited throughout the cough cycle by the second-order cough neurons, as were PRG populations (Fig. 4; perturbation 2). Although the latter connectivity remains speculative, the rostral dorsolateral pons is known to receive projections from airway rapidly adapting receptor relay neurons in the NTS (Ezure et al. 1991). The model generated realistic cough-like motor patterns (compare Fig. 6 to Fig. 7) in phrenic, lumbar, and laryngeal motoneurons, and exhibited activity profiles of functionally antecedent VRC and pontine neuron populations similar to those observed in vivo (Baekey et al. 2001; Shannon et al. 2000, 2004a,b).

Firing rate changes of pontine neurons during fictive cough elicited in vivo by mechanical stimulation of the intrathoracic trachea (mid-cervical to carinal region) are illustrated in Fig. 6 (data derived from Shannon et al. 2004a). Whether the PSR presynaptic inhibition of VRC respiratory-modulated inputs to PRG neurons is altered during cough remains unknown; the effect was blocked during simulated cough by an inhibitory connection from cough second-order neurons to Pump− neurons that project to the PRG to allow accentuated changes in activity in PRG neurons as observed in vivo.

The inspiratory phase of cough was elicited by activation of cough afferents that excited the second-order cough neurons. These neurons excited VRC I-Dec and I-Aug neurons, leading to an increased slope, amplitude, and duration of inspiratory motor (phrenic and inspiratory laryngeal, ILM) activity. Expiratory neurons were suppressed by the inhibitory actions of I-Dec and I-Aug neurons. The duration of the inspiratory phase was determined in part by I-Driver neurons and was terminated by

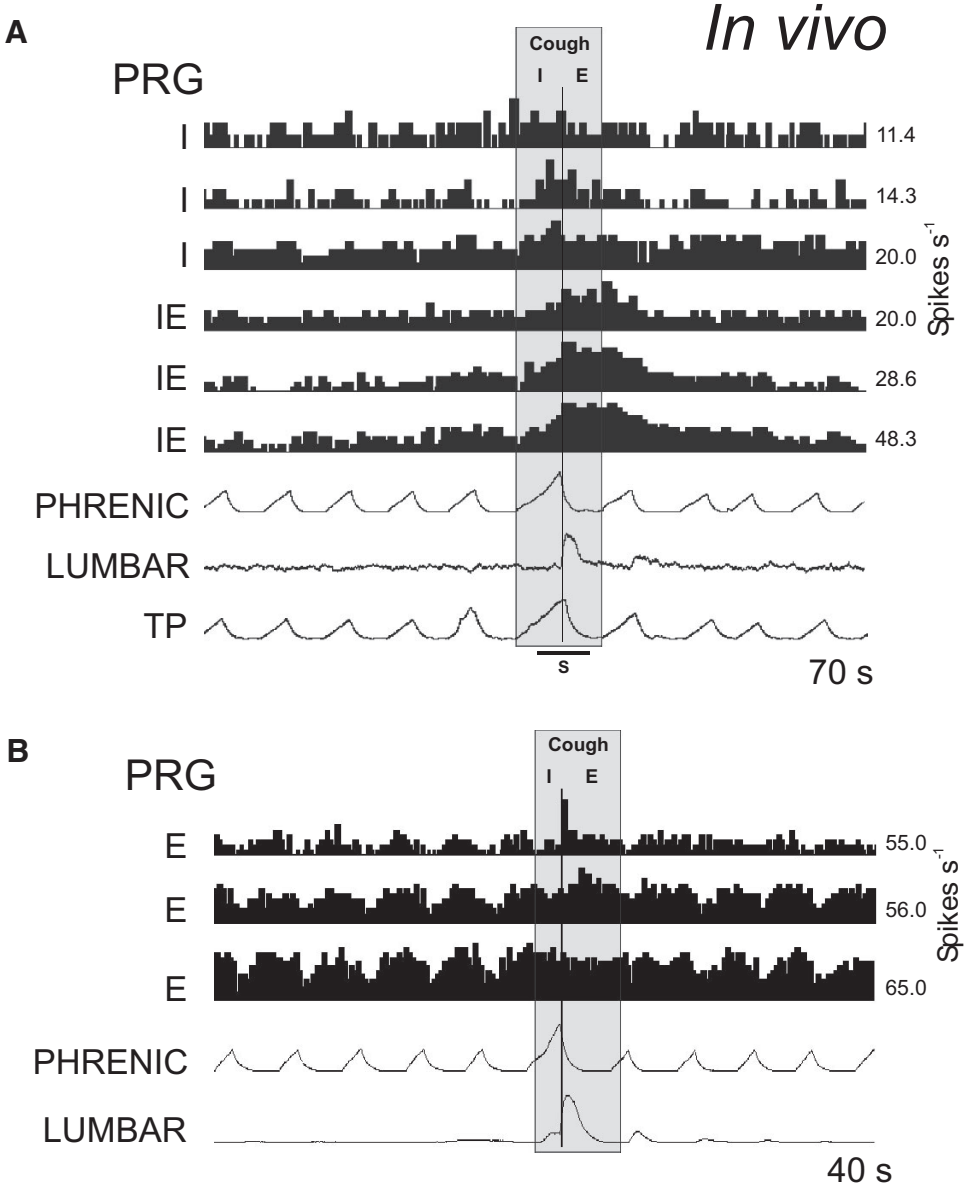

FIG. 6. Firing rate histograms from simultaneously recorded pontine respiratory group neurons during fictive cough elicited by mechanical stimulation of the intrathoracic trachea in a decerebrate neuromuscularly blocked cat. *A*: traces show control respiratory-modulated discharge patterns [3 inspiratory (I) and 3 inspiratory-expiratory (IE) phase-spanning neurons] and altered rates during the cough motor pattern defined by altered phrenic (inspiratory) and lumbar (expiratory) motoneuron activity. *B*: firing rates of 3 pontine respiratory group (PRG) expiratory neurons during fictive cough. Data in *A* and *B* are modified from Shannon et al. (2004a) and used with permission.

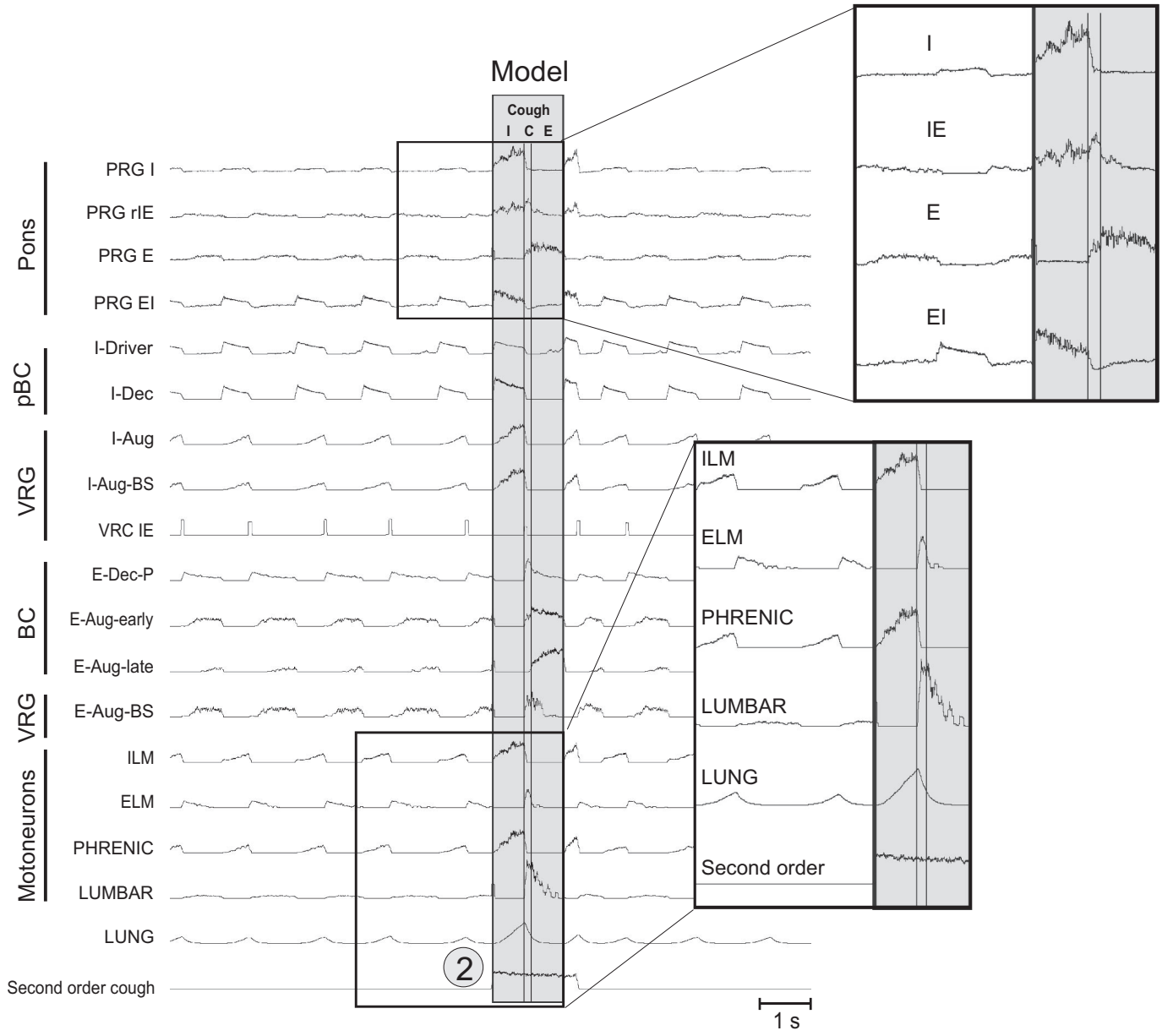

FIG. 7. Simulation with the extended model produced cough-like motor patterns. The simulated activities of phrenic, lumbar, and laryngeal motoneurons and functionally antecedent VRC and pontine neuron populations were similar to those observed in vivo. A fiber population consisting of 100 fibers, each with 100 excitatory synaptic terminals (see legend, Table A3 of the APPENDIX) with a synaptic strength of 0.02 was used to represent cough receptor excitation; each fiber had a firing probability of 0.05 at each simulation time step. This fiber population excited a second-order "cough" neuron population (Fig. 4); see Table A7 (APPENDIX) for properties of the cough population, Table A8 (APPENDIX) for details of connections with other populations, and the text for further details.

the onset of the inhibitory actions of E-Dec-P, E-Aug-early and VRC IE activity. This E-Dec-P and E-Aug neuron activity was due to a reduction in inhibition by I-Dec neurons and excitation by increased PSR-driven Pump+ cell and cough receptor activity.

The compressive (C) phase was brief and occurred near the end of the I phase; it was characterized by a large simultaneous increase in activity of E-Aug-BS, spinal E motoneurons (Lumbar) and expiratory laryngeal motoneurons (ELM). E-Aug-BS activity increased because of excitation by cough receptors and PSR Pump+ cells, reduced inhibition by I-Dec and subpopulations of E-Aug-early and E-Dec-P neurons, and postinhibitory rebound. The burst of ELM activity was due to excitation by E-Dec-P neurons, with the latter population's discharge enhanced by cough receptors and PSR, and enhanced postinhibitory rebound resulting from the cessation of previously enhanced I-Dec neuron activity. The compressive phase ended with a rapid decline in ELM discharge due to inhibition from E-Aug-late neurons that also inhibited the "residual" I-Aug-BS activity.

The expulsive phase of cough began with the sharp decline in ELM activity. E-Aug-BS neuron and lumbar activities continued to increase for a short time after the compressive phase. As the expiratory phase progressed, E-Aug-BS neurons and expiratory motoneurons had a *dec-*

rementing discharge pattern, shaped by the inhibitory actions of E-Aug-late neurons with activity that began after the onset of the E phase, and decreasing PSR activity.

The enhanced model with its incorporated PRG connectivity and pontine neuron discharge patterns similar to those observed in vivo (Fig. 6) provided a framework for the following hypotheses on roles of the pons in cough motor pattern generation.

First, the slope and peak activity of PRG I cells increases during the inspiratory phase of cough due to excitatory input from VRC I-Aug and I-Dec neurons. The PRG I neurons reciprocally excite VRC I-Aug neurons contributing to the augmented motor output. In addition to a cessation of inspiratory drive from the VRC, PRG I neuron activity is inhibited by VRC E-Aug neurons.

Second, PRG EI neuron firing rates rise sharply at the onset of the cough I phase and then decrement due to excitation from cough receptors, the pattern of excitation from VRC I-Dec neurons, and increasing inhibition by PRG IE neurons. This PRG EI activity, in turn, contributes to excitation of PRG rIE neurons, thus accelerating this recurrent inhibitory input. Both PRG EI and PRG I neurons excite VRC IE neurons. While activity of the latter population persists at the inspiratory-compressive phase transition in the model, its firing rate is diminished relative to control cycles. The termination of the inspiratory phase during cough in the model is thus due primarily to VRC E-Dec and E-Aug-early neurons.

Third, an increase in PRG IE neuron activity begins in the cough I phase and peaks near the transition of the inspiratory to compressive phase. The firing rate subsequently decrements during the expulsive phase. The inspiratory portion of the PRG IE neuron pattern is shaped by excitatory inputs from PRG I and EI neurons and cough receptors and inhibitory inputs from VRC I-Aug and I-Dec neurons. The pattern of the PRG IE neurons reflects increased excitation from VRC E-Dec neurons starting at the IE phase transition, along with increased inhibition from PRG E neurons, which contributes to the decrementing pattern during the expulsive phase. Excitatory projections from PRG IE neurons to VRC IE and E-Dec neurons contribute to the termination of the inspiratory phase; PRG EI neurons are also inhibited by PRG IE neurons.

Fourth, PRG E neurons generally have an augmenting pattern during control cycles. During cough, they reach peak firing rate during the early expiratory phase followed by a slowly or rapidly declining frequency. These discharge patterns result from excitatory drive from VRC E-Aug neurons and cough receptors. The increased activity in the early expiratory phase during cough is due to input from E-Aug-early neurons. In addition to the inhibition of PRG IE neurons, PRG E neurons inhibit VRC I-Dec neurons.

Modeling the effects of hypoxia on the respiratory motor pattern during NREM sleep

Our modeling efforts were coordinated with experimental investigation of changes in the activity of medullary respiratory neurons during hypoxia in NREM sleep in the cat (Lovering et al. 2006). Activity of 120 neurons was analyzed. In normoxia during NREM sleep, inspiration develops slowly with peak airflow rates occurring at the end of the breath. In expiration, a high airflow rate occurs in early expiration and gradually decreases throughout the phase. These patterns are reversed in hypoxia. Specifically, a high inspiratory airflow rate occurs at the beginning of the breath; it is maintained or decreases as the breath proceeds. Similarly, the pattern of airflow during expiration in hypoxia is opposite to the pattern in normoxia. That is, expiratory airflow is minimal at the beginning of expiration but increases at the end of expiration (Lovering et al. 2003). In addition to the changes in airflow profile, the rate of breathing increases in hypoxia, primarily because of a reduction in the duration of inspiration.

Changes in neuronal activity pattern profiles in NREM sleep during hypoxia with respect to the activity profiles observed during normoxia are shown in Fig. 8A (derived from Lovering et al. 2006; used with permission). The activity patterns are representative of the predominant responses of the respective cell types, but there were cells of each type that responded differently. The majority of I cells were more active in hypoxia than normoxia, and in the case of I-Aug neurons, the pattern of activity was a step increase in activity followed by a ramping increase to peak activity at the end of inspiration. These changes could cause the change in inspiratory airflow profile in hypoxia. Similarly, the observation that decrementing, augmenting, and inspiratory-expiratory neurons increased their activity sooner and ended their activity more abruptly during inspiration in hypoxia during NREM sleep could explain the increased rate of breathing.

To simulate the effects of hypoxia during NREM sleep an additional drive ("hypoxia," imitating an increased input from the peripheral chemoreceptors) was incorporated in the model. This additional drive was applied to all neuron types (Fig. 8*C;* perturbation 3): expiratory (E-Aug-late, E-Aug-early, E-Aug-late-HT, E-Aug-BS, E-Dec-P, and E-Dec-T), inspiratory (I-Dec, I-Aug, I-Aug-BS), IE-VRG, and I-Driver. Using our extended model, we were able to find a set of synaptic weights representing the effects of chemoreceptor activity with hypoxia to these neuronal populations (see hypoxia effect population properties and connections, Tables A7 and A8, APPENDIX) that allowed the model to closely reproduce changes in profiles of different medullary respiratory populations observed in NREM sleep during hypoxia (Fig. 8*B*). Our simulations were also able to reproduce changes in timing of neuronal activities similar to those seen in vivo. In particular, the earlier onset of activity in the E-Dec population and increased firing rates of the VRC IE neurons (not shown), both of which are inhibitory to inspiratory neurons, caused a decrease in the duration of inspiration.

Prediction of possible co-expression of multiple rhythms under certain conditions

As shown in the preceding text, the removal of the pons in the initial model (eliminating PRG modulation of the respiratory network behavior) resulted in a I_{NaP}-dependent gasping-like motor activity originating in the I-Driver population (Fig. 2*D*). Similarly, the loss of pontine input in the extended model (see Fig. 4, perturbation 4) also switched the I-Driver population to an endogenous bursting state, in

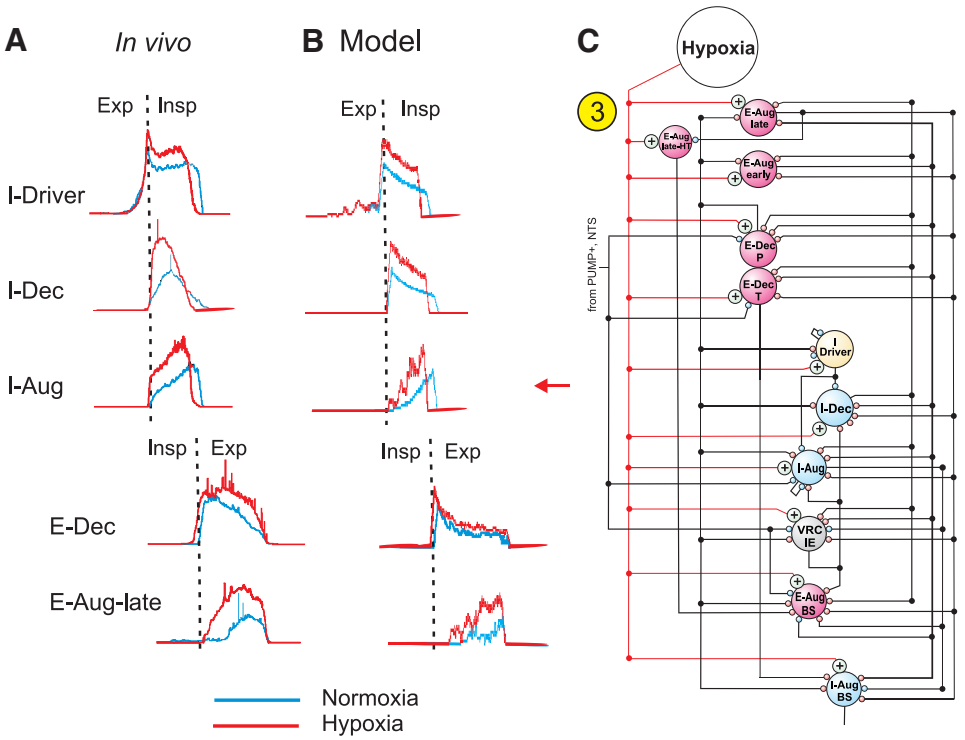

FIG. 8. Modeling effects of hypoxia on the respiratory motor pattern during non-random eye movement (NREM) sleep. *A*: changes in the integrated profiles of activity of different respiratory neurons during hypoxia (red traces) vs. normoxia (blue) from a coordinated in vivo study by Lovering et al. (2006) and used with permission. *B*: activity profiles in different medullary model populations closely reproduced changes found during hypoxia in NREM sleep. Hypoxia was simulated by incorporation of additional source of excitatory drive. *C*: schematic shows excitatory inputs that simulated a "hypoxic drive" to the indicated VRC populations (perturbation 3). A fiber population consisting of 100 fibers, each with 100 excitatory synaptic terminals with a synaptic strength of 0.025 was used to represent chemoreceptor drive; each fiber had a firing probability of 0.05 at each simulation time step. This fiber population, in turn, excited a second-order "Hypoxia" effect neuron population; see Table A7 (APPENDIX) for properties of this population and Table A8 (APPENDIX) for details of connections with other populations represented in *C*. See text for further details.

which it can drive rhythmic activity in the entire network (Fig. 9, *A* and *B, left*). Simultaneously, the activity in other inspiratory and expiratory populations was reorganized (Fig. 9, *A* and *B, left*). The VRC I-Aug and I-Dec populations exhibited increased activity early in each resulting gasping-like burst. The prolongation of the I-Dec population's interval of declining activity until the subsequent expiratory phase reflected the balance of synaptic strengths in the extended model and the accommodative properties of the I-Dec population.

Importantly, a subsequent suppression of expiratory activity (in the E-Dec-P, E-Aug-early, and E-Aug-late populations) did not perturb stable oscillations of phrenic nerve activity driven by pacemaker activity in the I-Driver population (Fig. 9*A, right*), whereas a suppression of I_{NaP} in the I-Driver population (by setting the maximal conductance for NaP channels in all neurons of the population to 0) stopped rhythm generation (not shown), confirming that the rhythm originates in this population and is based on I_{NaP}. Alternatively, when the I-Driver population was inhibited instead, the phrenic motor output was suppressed, but the network continued generation of rhythmic activity produced by network interactions (Fig. 9*B*). This result extended the earlier observation from the initial model that a network-based rhythm can be generated even in the absence of an I-Driver population, and led to the prediction that the network can be configured with more than one rhythm-generating mechanism (see also Rybak et al. 2007a; Smith et al. 2000, 2007).

A gasping-like activity produced in the model by removal of PRG inputs and reduction of excitatory drive is shown in Fig. 10*A* (*left*). This activity with decrementing gasp-like bursts in phrenic nerve is similar to that observed during gasping in vivo (Solomon 2000) and in situ (St-John and Paton 2003b). Using our model, we have shown that with a subsequent tonic re-excitation of the VRC network, the model may continue generating pacemaker-driven gasp-like bursts, but with a second, network-generated activity superimposed on it, resulting in a "burst-ramp" motor pattern (Fig. 10*A, right*). The phrenic pattern in one cycle (marked by dashed red ellipse) is shown enlarged in Fig. 10*B*.

During severe brain hypoxia and initial re-oxygenation in vivo, the eupneic pattern of inspiratory motor output is replaced by gasping and/or augmented bursts (i.e., a eupneic-like burst terminated by a gasp-like discharge) (Solomon 2000). Our simulation results allow the suggestion that hypoxia-induced gasps are generated by a dynamically "reduced" network, involving a I_{NaP}-dependent intrinsic mechanism in the pre-BötC (see Paton et al. 2006; Rybak et al. 2002, 2004a, 2007a; Smith et al. 2007), and that recovery from hypoxia-induced gasping may be associated with transitional states, with gasp-like bursts superimposed on a re-emerging network-generated ramp-like inspiratory pattern (Fig. 10*C*). These modeling results motivated new in vivo experiments to address this hypothesis.

To test this prediction, activity of different respiratory neurons within the VRC and efferent phrenic (fictive) motor patterns were monitored in vivo during control fictive breathing, followed by hypoxia (gas mixture of 5% O_2-95% N_2) and then by re-oxygenation (Solomon 2000, 2002) in vagotomized, decerebrate, neuromuscularly blocked, thoracotomized, and artificially ventilated cats. Parallel recordings of multiple single neuron spike trains were made with a multi-electrode array. In 9 of 11 experiments, the patterns of phrenic nerve activity during severe brain hypoxia and recovery were similar to those resulting from the simulations described in the preceding text: activity progressed from fictive gasp-like bursts to ramp activity with superimposed bursts to augmenting discharge patterns similar to those observed during the control period.

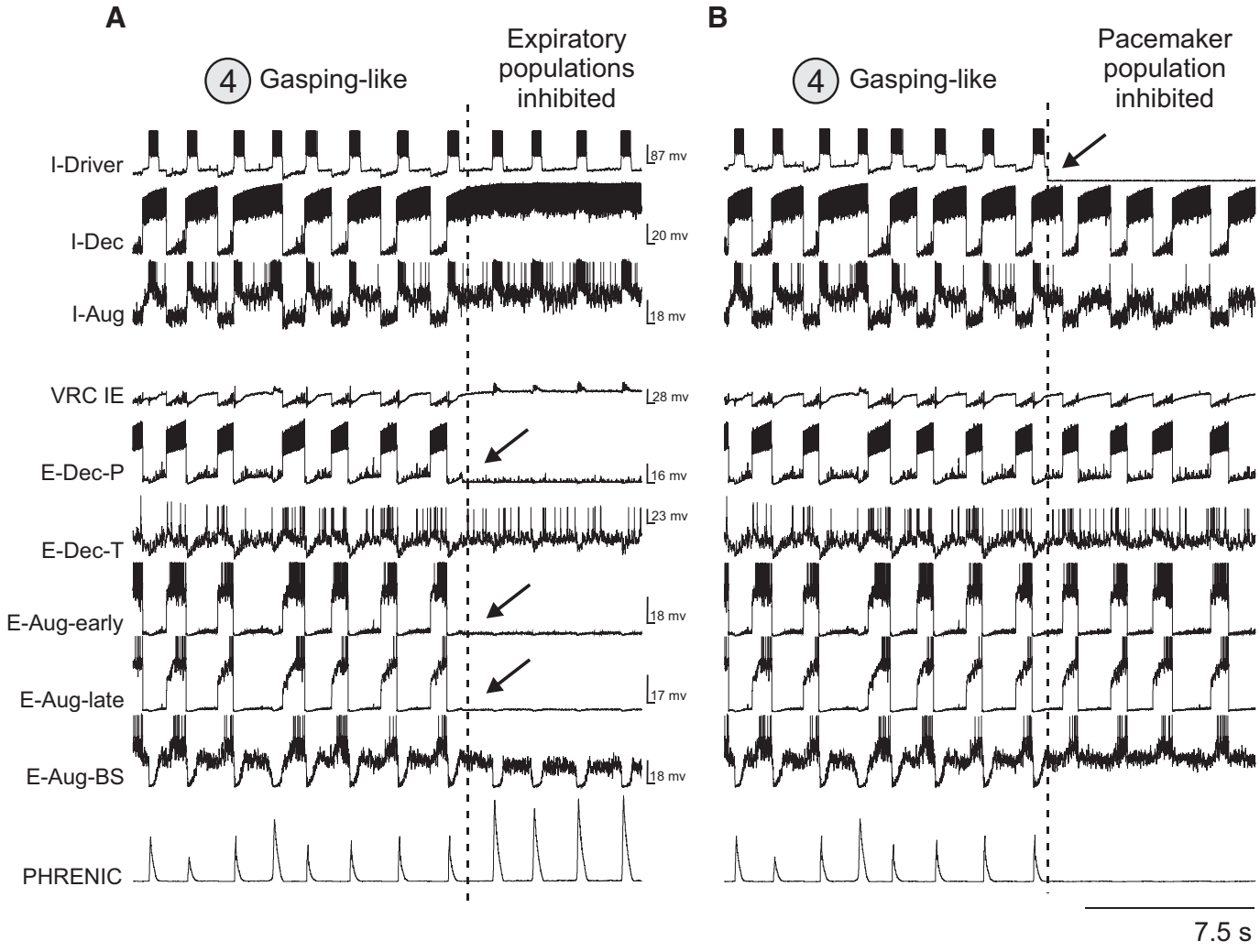

FIG. 9. Gasping-like pattern (in both *A* and *B*) was produced by PRG removal (perturbation 4—circled; see also in Fig. 4). The I-Driver population in this case operates in the endogenous pacemaker mode and drives respiratory oscillations in the network and motor output. Membrane potential traces (independently scaled) of a single I-Driver neuron and a subset of other representative respiratory neurons are shown in both *A* and *B*. *A*: subsequent suppression of ventral respiratory column (VRC) expiratory neuron populations (vertical dashed line) did not suppress endogenous gasping-like activity in the I-Driver population and phrenic motor output. *B*: 2nd simulation run with initial activity the same as in *A*. Inhibition of I-Driver population (vertical dashed line) eliminated the phrenic gasp pattern; however, interactions among remaining active VRC populations were sufficient to generate rhythmic activity within the network.

The firing rates of 10 simultaneously monitored single neurons and phrenic nerve activity recorded during a control period are shown in Fig. 11*A*. This sample included VRC neurons with I-EI (putative I-Driver), I-Aug, IE, E-Dec, and E-Aug discharge patterns (see Fig. 11*G*). Hypoxic exposure in this carotid body-intact preparation first produced an excitatory response followed by hypoxic depression (not shown). Subsequently, during recovery from the depression, phrenic gasp-like bursts were observed, which were associated with corresponding activity in the I-EI neuron and a subset of I neurons (Fig. 11*B*). Some spike train burst peaks were observed that preceded phrenic bursts, while others were synchronized with or followed peak phrenic activity.

The posthypoxic "recovery" was first associated with the re-emergence of E-Aug neuron activity (Fig. 11*C*) followed by spiking in the E-Dec neurons (Fig. 11, *D–F*). After recovery, an augmenting eupneic-like phrenic pattern was fully re-established (Fig. 11*F*). However, this recovery of the eupneic phrenic pattern went through intermediate stages in which gasp-like decrementing bursts were superimposed with re-emergent augmenting bursts (Fig. 11, *D* and *E*). The evolution of integrated phrenic discharge profiles is shown in Fig. 11*H,* which demonstrates that during the recovery phase distinct phrenic motor patterns evolved, alternating in successive cycles during some intervals. The phrenic pattern marked by a dashed red ellipse was similar to the phrenic activity profile from the model shown in Fig. 10*B.* As the pattern returned to that observed during the control period, two profiles alternated, with a burst apparently superimposed on a control-like ramp (dashed red line; see *bottom 2 profiles*). This sequence of simultaneously recorded discharge patterns suggests that components of a distributed neural network active during eupnea can be coordinated with a functionally "simplified" and distinct mechanism that generates gasps and augmented burst activity during recovery from severe brain hypoxia as predicted by the model.

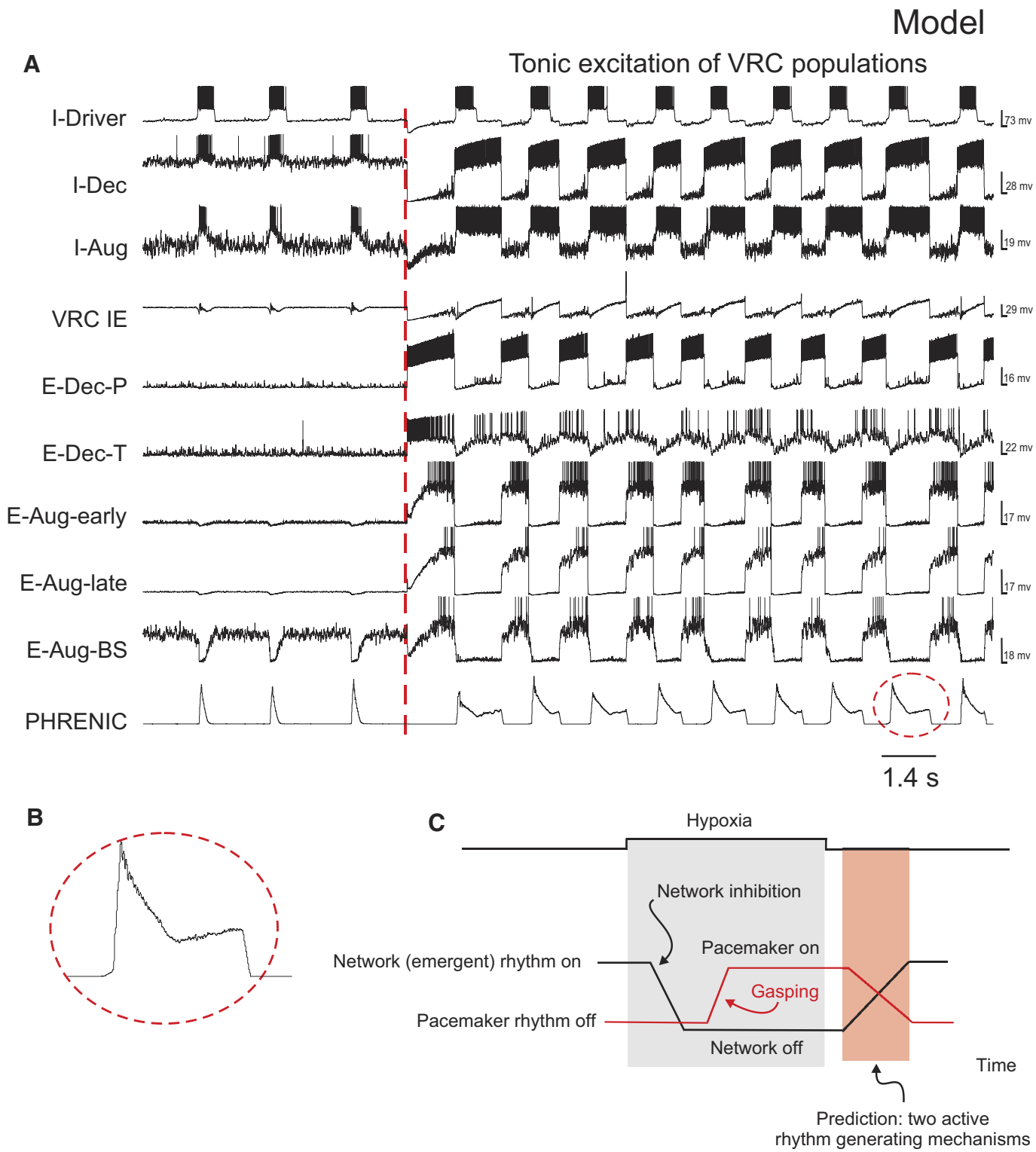

FIG. 10. Model prediction of possible co-expression of gasp-augmenting burst and eupneic-like ramp patterns with progressive alteration in tonic excitation of VRC populations. *A, left*: gasp-like phrenic activity pattern and traces of representative membrane potentials from single representative neurons after PRG removal and reduced excitation of E-Aug-BS,VRC IE, I-Aug, I-Dec, E-Aug-late, E-Aug-early, E-Dec-P, and E-Dec-T populations. A "burst–ramp" type phrenic motor pattern emerged with the onset of tonic re-excitation of the VRC network populations (red dashed line), together with additional I-Aug excitation mediated by an excitatory "Biasing" population (see Table A7, APPENDIX for parameters). *B*: detail from *A* shows a "burst–ramp" type pattern during an inspiratory phase. *C*: summary of a prediction from the model showing that 2 active rhythm-generating mechanisms can be simultaneously expressed during recovery from hypoxic gasping. See text for details.

DISCUSSION

This study was motivated by the need to develop a model framework for investigation of the role of the pontine respiratory group and its functional connectivity with neurons in other brain stem regions involved in generating and shaping respiratory motor patterns. An additional goal was to use the model for generating predictions for network mechanisms responsible for the specific changes in neuronal discharge profiles and motor patterns observed during various perturbations, including brain stem lesions, evoked cough, and during state-dependent motor pattern alterations during sleep (Lovering et al. 2006; Shannon et al. 1998, 2000, 2004a). The results of modeling also led us to the prediction that a "burst-ramp" motor pattern can be generated during the re-emergence of respiratory network activity after hypoxia-induced gasping, which we tested experimentally.

Our approach consisted of model development in coordination with in vivo experiments guided by both model predictions and gaps in knowledge highlighted by the models. In our initial model, the core VRC circuit incorporated a large set of functional connections based on in vivo dual neuronal recordings analyzed with either extracellular spike train cross-correlation data or spike-triggered averages of synaptic potentials. However, most connections between VRC and PRG populations and within the PRG were ad hoc, which provided a basis for addressing several model-guided hypotheses. These hypotheses were then supported by subsequent experimental work (Segers et al. 2008). The results of our experimental studies supported some of the hypothesized functional interactions (while rejecting others) and provided evidence for other connections that were included in the extended model.

The extended model represents a new instantiation of the motivating hypotheses that both paucisynaptic inputs from VRC populations and intrinsic pontine interactions shape the respiratory modulation of PRG neurons and that PRG populations participate in phase switching and the reconfiguration of the respiratory network under different conditions. The resultant model has demonstrated robust rhythm-generating properties and suggests the existence of at least two (network-based and pacemaker-driven) rhythmogenic mechanisms, which may respectively dominate under different conditions (see also Paton et al. 2006; Rybak et al. 2002, 2004a, 2007a; Smith et al. 2000, 2007) and, as we show in this study, can be co-expressed during state-transitional periods.

Results from the present models on the re-initiation of rhythmic activity without I-Driver neurons replicated previous simulation results (Balis et al. 1994). These simulations predicted that complete suppression of I-Driver activity can produce transient apnea and that rhythmogenesis can, in principle, reappear without activity in that population. Transient apneas following ablation of the pre-BötC (St-Jacques and St-John 1999) and ataxic breathing patterns following selective lesions of pre-BötC neurons that expressed neurokinin-1A receptors (Gray et al. 2001) are consistent with this hypothesis.

Changes in chemical drive could potentially contribute to such a recovery from the apnea following inactivation of the I-Driver population. Experimental observations (Morris et al. 1996) support a distinct but parallel chemoreceptor regulation of phase timing and drive. Putative I-Driver neurons were observed to be influenced differently than caudal presumptive premotor inspiratory neurons by selective stimulation of peripheral chemoreceptors. The duration of the active phase of the rostral I-Driver neurons decreased with little or no increase in firing rate, whereas the caudal I-Aug neurons increased their firing rate.

Preliminary results from multi-array recordings from in vivo preparations similar to those reported herein have shown that I-EI (I-Driver-like), I-Aug, and I-Dec neurons may exhibit concurrent decreases in firing rate during hyperventilatory (hypocapnic) apnea, while E-Aug neuron activity may become tonic (not respiratory modulated) and increase (Nuding et al. 2005). These results are consistent with earlier observations of tonic expiratory motoneuron activity during hypocapnic apnea and reciprocal inhibition of tonic inspiratory and expiratory activity with changes in chemical drive (Sears et al. 1982).

Strengths and limitations of approach

In this study, we used a computational model of a spatially compartmentalized brain stem respiratory network as a tool to guide coordinated complementary experiments. In turn, the model was iteratively constrained by data obtained from the in vivo experiments (Segers et al. 2008). The new model focused on the role of the PRG and interactions between the PRG and VRC. It also consolidated disparate observations and hypotheses on the organization of the brain stem respiratory network, including spatial organization of the brain stem respiratory network and the existence of multiple state-dependent mechanisms for respiratory rhythm generation (Rybak et al. 2007a; Smith et al. 2007), reorganization of rhythm-generation mechanisms during the transition from eupnea to gasping (Paton et al. 2007), the important role of I_{NaP}-dependent mechanisms within the pre-BötC (Smith et al. 2000), and the role of the PRG in control of timing of respiratory phase transitions and phase durations (Cohen and Shaw 2004; Haji et al. 2002; Okazaki et al. 2002). Also, our simulations led to an interesting prediction on the reconfiguration of the respiratory network and the re-emergence of the eupneic pattern following hypoxia, which was confirmed experimentally.

Further development of the model will require more data on connectivity within the respiratory network. For example, the current model has not considered the effects of PSR activation on the activity of different PRG neurons (Dick et al. 2002) other than previously suggested presynaptic inhibition of VRC respiratory inputs (Feldman et al. 1976; Kubin et al. 2006). Pump–cell-mediated presynaptic inhibition remains speculative and other network interactions may contribute to changes in pontine respiratory-modulated activity following vagotomy (Dick et al. 2008). The model has yet to incorporate proposed connectivity of the VRC with other modulatory brain regions such as the medullary raphé nuclei (Lindsey et al. 1994) or with the RTN/parafacial nucleus, a region with proposed roles in rhythm generation (Feldman and Del Negro 2006; Onimaru et al. 2006; however, see Fortuna et al. 2008) and chemoreceptor function-

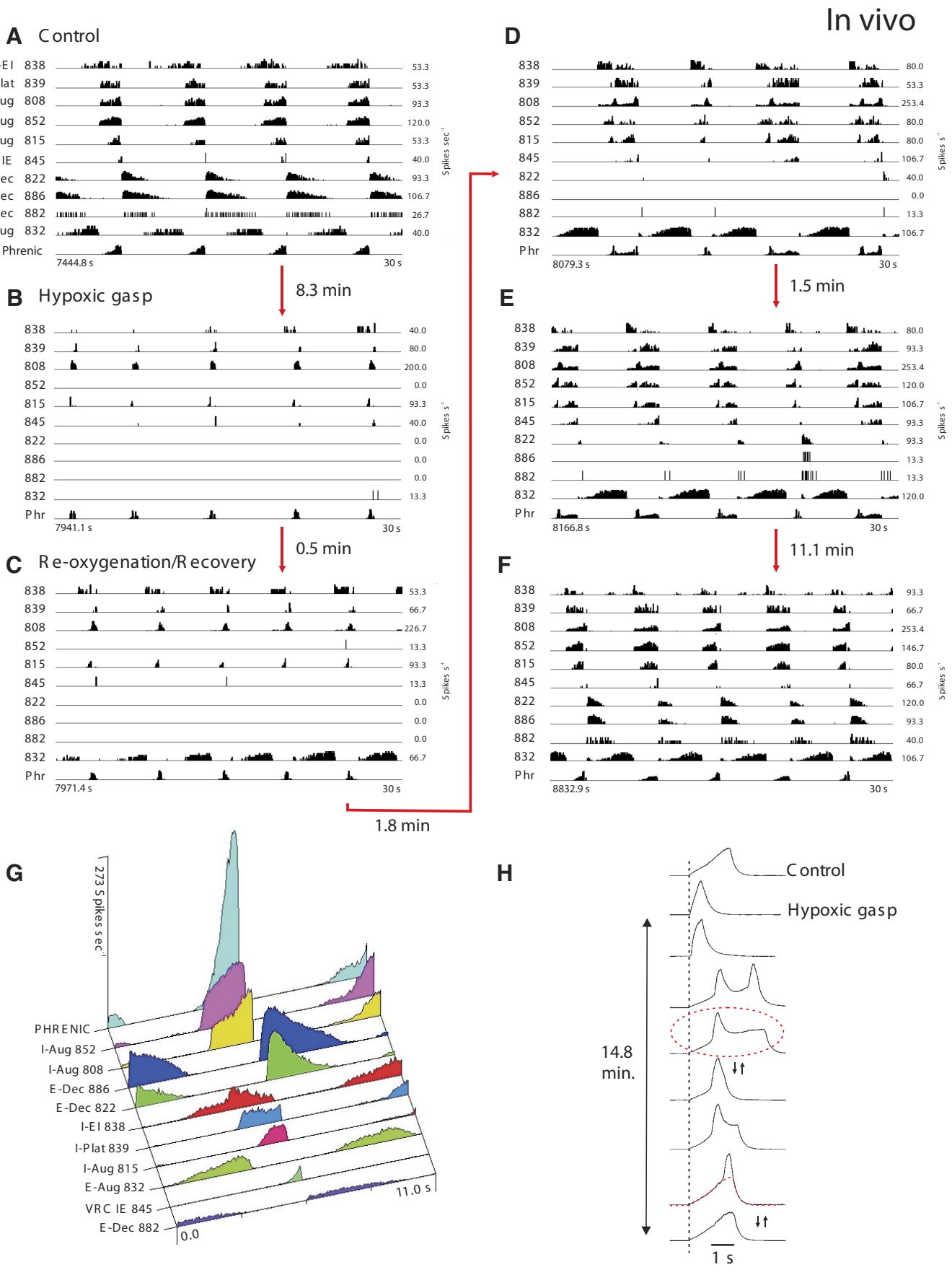
In vivo
A Control
I-EI 838
I-Plat 839
I-Aug 808
I-Aug 852
I-Aug 815
VRC IE 845
E-Dec 822
E-Dec 886
E-Dec 882
E-Aug 832
Phrenic
7444.8 s
30 s
Spikes sec⁻¹
8.3 min
B Hypoxic gasp
7941.1 s
0.5 min
C Re-oxygenation/Recovery
7971.4 s
1.8 min
D
8079.3 s
1.5 min
E
8166.8 s
11.1 min
F
8832.9 s
G
273 Spikes sec⁻¹
PHRENIC
I-Aug 852
I-Aug 808
E-Dec 886
E-Dec 822
I-EI 838
I-Plat 839
I-Aug 815
E-Aug 832
VRC IE 845
E-Dec 882
0.0
11.0 s
H
Control
Hypoxic gasp
14.8 min.
1 s

ality (Mulkey et al. 2004). We note that preliminary results from large-scale multi-array recordings suggest a rich set of connections between the raphé nuclei and the pontomedullary network, including "indirect" paths between the PRG and VRC via intervening brain stem midline neurons (Nuding et al. 2006).

Changing respiratory pattern with brain stem transections

Our models were able to reproduce early experimental data on breathing pattern transformation following brain stem transections in cats in vivo (Lumsden 1923; St-John 1998). Specifically similar to these in vivo experiments in cats, a removal of rPons in our models converted the eupneic three-phase pattern to "apneusis" and the complete elimination of the pons (additional removal of cPons) replaced apneusis with a gasping-like pattern.

Interestingly, Rybak et al. (2007a) and Smith et al. (2007) have recently performed a detailed investigation of changes in the rhythmogenic mechanisms and pattern of phrenic activity in an in situ perfused rat brain stem–spinal cord preparation following brain stem transections that were sequentially shifted in the rostral-to-caudal direction. They have clearly demonstrated that with removal of the pons, the normal three-phase respiratory rhythm is transformed to a two-phase rhythm, exhibiting a square-wave pattern of phrenic activity, and that the transition to a one-phase "gasping-like" rhythm occurs with more caudal brain stem transections. These data obtained in the in situ perfused rat preparations differ from the earlier data obtained in vivo in cats (Lumsden 1923; St-John 1998), in which a gasping-like pattern occurred after removal of the pons. Our coordinated experimental studies did not include brain stem transections. However, they were performed in cats in vivo. Therefore although our models could be re-adjusted to fit Rybak et al. (2007a) and Smith et al. (2007) data, we preferred to relate our models to the earlier cat data. At the same time, we note that generally our model has no conceptual contradiction with the Rybak et al. (2007a) and Smith et al. (2007) results. Indeed, certain differences between the preparations (in vivo cat versus in situ perfused rat) exist. The two-phase pattern described by Rybak et al. (2007a) and Smith et al. (2007) looks similar to (and maybe is) an apneustic pattern: it is characterized by a prolonged duration of inspiration and a square-wave shape of phrenic bursts. The phrenic pattern during apneusis in rats is not the same as in cats; the inspiratory duration is not as long and expiratory duration is rather normal or increased but not reduced as in cat (e.g., see Fung and St-John 1995; Morrison et al. 1994; Rybak et al. 2004a). Moreover, the apneustic phrenic pattern in the rat looks similar to the two-phase pattern described by Rybak et al. (2007a) and Smith et al. (2007). The latter studies also demonstrated that with more caudal brain stem transections (when drives from structures rostral to BötC–pre-BötC were reduced), the phrenic pattern changed from an "apneustic" two-phase pattern to a "gasping-like" one-phase pattern. Hence, the major difference may be the point at which the system switches from an apneustic two-phase pattern to a one-phase gasping-like pattern: with the transection at the pontine-medullary junction (Lumsden 1923; St-John 1998) or with more caudal brain stem transections (Rybak et al. 2007a; Smith et al. 2007). This difference may reflect differences between the preparations, different consequences of transections, and/or different metabolic conditions within the preparations. For example, it may be the case that in rats (in contrast to cats), drive from RTN to more caudal structures (when RTN is fully intact) is still strong enough to maintain a two-phase rhythm even when pons is removed. Hence we do not consider this difference to be a critical conceptual contradiction.

Reconfiguration of the network during cough

The extended model presented herein can reproduce firing profiles and changes in the respiratory motor pattern observed in vivo in response to various perturbations, including those evoked during cough. The discharge profiles of several PRG neuron populations during cough were similar to those observed in antecedent experimental work (Shannon et al. 2004a). The in vivo work had suggested that pontine neuron discharge patterns during cough reflect, at least in part, inputs from the ventral respiratory column because the response patterns of the pontine I, IE, and E cells were similar to those observed in subgroups of medullary VRC neurons with comparable control discharge profiles (Shannon et al. 1998, 2000). The present results suggest a specific network configuration and that both intra-pontine interactions and connections between the pons and VRC contribute to cough motor pattern dynamics during this airway defensive behavior. Further research is needed to identify the routes through which cough receptors act to evoke reconfiguration of the network in vivo (Baekey et al. 2003; Bolser et al. 2006; Shannon et al. 2004a,b).

Patterns and responses observed during hypoxia and sleep

Hypoxia profoundly alters the pattern of breathing in intact unanesthetized animals (Lovering et al. 2003; Solomon 2003). Inspiratory activity increases during hypoxia in several ways. First, the profile of diaphragmatic activity changes from an augmenting ramp to basically a square wave, and, second, this activity persists, although diminished, into expiration, presumably to brake expiratory airflow. Also the rate of breathing increases because of a decrease in the duration of inspiration. Studies of single respiratory neurons in unanesthetized cats have demonstrated that a majority of neurons in both inspiratory and expiratory categories exhibit increased activity during hypoxia in NREM sleep (Lovering et al. 2006). Specifically, the following average increases were measured during hyp-

FIG. 11. In vivo VRC neuronal activity profiles during control, hypoxic gasping, and recovery. *A–F*: firing rates of 10 simultaneously recorded VRC neurons and efferent phrenic nerve activity during the prestimulus control period (*A*), hypoxia-induced gasp-like activity (*B*), and re-oxygenation (*C–F*). *G*: control respiratory cycle-triggered histograms for neurons in *A;* 37 cycles averaged. One inspiratory neuron had a relatively uniform firing rate during the inspiratory phase and was designated "I-plateau" (I-Plat); *H*: integrated phrenic nerve activity profiles detail control, gasping, and a return to eupneic-like phrenic patterns with superimposed augmented bursts. Pattern with dashed line ellipse is similar to the phrenic activity profile observed in model simulations as shown in Fig. 10. See text for details.

oxia: I-Dec (183%); I-Aug (154%); I (155%); E-Dec (230%), E-Aug (191%), and E (136%).

Therefore to simulate the effect of hypoxia, an additional excitatory input to all VRC neurons was included in the model. Based on the preceding experimental data, both I-Dec and E-Dec populations were excited more strongly than the other populations (the synaptic weights to these populations were larger; see Table A8, APPENDIX). This allowed us to reproduce the alternations of discharge patterns of major VRC neuronal types like those recorded in vivo. Our simulations also led to the prediction that the increased rate of breathing observed in the intact animal's response to hypoxia can be explained by earlier and increased E-Dec and IE activity (Batsel 1965; England et al. 1995; Lovering et al. 2006).

Coupled rhythm-generating processes and gasping

In the model, a gasping-like activity associated with removal of PRG inputs became superimposed on a second network-generated rhythm during subsequent tonic re-excitation of the VRC network, resulting in a "burst-ramp" motor pattern. This result suggested that two rhythmogenic mechanisms were engaged and could operate simultaneously: one based on network interactions and the other relying on conditional endogenous pacemaker properties in the pre-BötC I-Driver population. Specifically, the model predicted that such a co-expression of these mechanisms could occur during the transition from gasping to eupnea and be seen in the phrenic motor output.

Two different views on the role of medullary pacemaker neurons in the generation of eupnea and gasping have recently been debated (Paton and St-John 2007 vs. Ramirez and Garcia 2007; see also Rybak et al. 2007b). These concepts differ in their view on the role of pacemaker neurons in respiratory rhythm generation during eupnea but agree that pacemaker neurons are essential for generation of gasping. Recent studies by Rybak et al. (2007a) and Smith et al. (2007) specifically addressed in detail the issue of the roles of pre-BötC neuronal intrinsic bursting properties in different network states and provided a possible biophysical mechanism to explain why these properties may not be involved during generation of the eupneic pattern (i.e., under high tonic excitatory drive, I_{NaP} is essentially inactivated because of its voltage-dependent inactivation properties). Our model is also consistent with the idea of an essential role of pacemaker-generating activity during gasping. As in the previous models of Rybak et al. (2004a, 2007a) and Smith et al. (2007), during eupneic conditions the I-Driver population in the model operates in a nonendogenous bursting state without an involvement of endogenous pacemaker properties. The complete suppression of the pre-BötC I-Driver population can lead to apnea. However, our simulation shows and predicts that a subsequent increase in tonic excitation to key network elements can re-establish a eupneic-like pattern.

This prediction and the involvement of a functionally "reduced" network in the generation and transmission of the gasping motor pattern were subsequently supported by large electrode array recordings in coordinated in vivo experiments. Our approach exploited the well-established sequence of hypoxia-induced respiratory drive depression followed by apnea, gasping, and then recovery with re-oxygenation in decerebrate and anesthetized animal models (Solomon 2000; St-John and Paton 2003a,b). The results of our in vivo studies of hypoxia are also consistent with the hypothesis that in addition to direct motor output, gasp-producing neural networks operate to reactivate the respiratory network after hypoxic depression (Eisenberg 2006; Harper et al. 2000; Thuot et al. 2001). Inspiratory activity during gasping could "prime" or activate inspiratory neurons that participate in the re-emergence of the more distributed network-based respiratory pattern. Because we did not try to block NaP channels in the pre-BötC (which would be difficult to do in cats in vivo), we cannot confirm that the gasp-producing mechanism is I_{NaP}-dependent. However, based on previous studies in rats (Paton et al. 2006), we suggest that this intrinsic bursting mechanisms relies on I_{NaP}-dependent properties of the pre-BötC neurons.

Future directions

Further development of the model in conjunction with ongoing and future experimental studies of neuronal connectivity in the respiratory brain stem is likely to be fruitful. There is already a large body of experimental data on correlational linkages among neurons of the medullary raphé nuclei and the VRC (Arata et al. 2000; Lindsey et al. 1994, 1998; Nuding et al. 2006), and the raphé has been proposed as a site for transforming and transmitting information from various external and internal sensory systems (Feldman et al. 2003) and cardio-respiratory coupling (Morris et al. 2007) and for contributing to the induction and expression of long-term facilitation (LTF), a type of respiratory memory (Millhorn 1986; Mitchell and Johnson 2003; Morris et al. 2003). The model does not yet incorporate modifiable synapses or other mechanisms for generation of respiratory LTF (Morris et al. 2003; Neverova et al. 2007).

As noted in the preceding text, other neuronal populations of interest include those of the RTN (Feldman and Del Negro 2006; Mulkey et al. 2004; Onimaru et al. 2006), lateral tegmental field (Orer et al. 2006), and nonrespiratory modulated neurons adjacent to and intermingled with the neurons of the VRC (Segers et al. 2008). These sites are putative sources of network modulation and may participate in reconfiguring the network, for example, during evoked respiratory-related behaviors such as cough (Bolser et al. 2006).

The present modeling studies on network reconfiguration were confined to simulated "lesions" and physiological perturbations. The representation of such an expanded network in three-dimensional brain stem coordinate space will allow further model development and simulations of various brain stem lesions and other physiological and pharmacological perturbations that generate various reproducible alterations of the respiratory motor pattern. We also anticipate additional information on details of model network dynamics from the method of two-dimensional plotting of the distances in phase space between past and future states of the models (and of multineuronal data) in relation to a sliding reference point (Dunin-Barkowski et al. 2006). Finally, efforts to address other important questions about the role of the pons in coordinating laryngeal and diaphragmatic motor activities which typify eupneic and adaptive patterns of breathing will benefit from extending the model to include representations of the airways, lungs, and respiratory muscles.

APPENDIX A

TABLE A1. *Population parameters for initial model represented in Fig. 1*

Population	Size	Resting Threshold, mV	THO Variability, mV	Membrane Time Constant	Post-Spike Increase in G_K^+	Post-Spike G_K^+ Time Constant, ms	Adaptation Threshold Increase	Adaptation, ms	Noise Amplitude	DC, mV
Variable names	*N*	*THO*		*TMEM*	*B*	*TGK*	*C*	*TTH*		
PRG I	100	10.0	1.0	9.0	20.0	7.0	0.0	500.0	0.9	0.0
PRG rIE	100	10.0	1.0	9.0	20.0	7.0	0.0	500.0	0.9	12.0
PRG cIE	100	10.0	1.0	9.0	20.0	7.0	0.0	500.0	1.0	5.0
PRG E	100	10.0	1.0	6.0	27.0	2.5	0.0	500.0	0.9	0.0
PRG E-Other	100	10.0	1.0	9.0	20.0	7.0	0.0	500.0	0.9	20.0
PRG EI	100	10.0	1.0	9.0	20.0	7.0	0.0	500.0	0.9	0.0
PRG NRM+	100	10.0	1.0	9.0	20.0	7.0	0.0	500.0	0.03	25.0
PRG NRM−	100	10.0	1.0	9.0	20.0	7.0	0.0	500.0	0.09	15.0
I-DRIVER	300					see Table A2				
I-Dec	300	10.0	1.0	6.0	25.5	6.63	0.5	500.0	0.1	28.0
I-Aug-BS	300	10.0	1.0	6.0	25.0	3.8	0.0	5000.0	0.5	5.0
VRC IE	99	10.0	1.0	9.0	5.6	5.0	0.0	1000.0	0.54	7.0
E-Dec-P	99	8.0	1.0	9.0	27.0	2.5	0.8	2000.0	0.1	7.0
E-Dec-T	300	8.0	1.0	9.0	27.0	2.5	0.8	2000.0	0.06	16.5
E-Aug-early	300	10.0	1.0	6.0	27.0	2.5	0.0	500.0	0.1	21.0
E-Aug-late	300	10.0	1.0	9.0	27.0	2.5	0.0	500.0	0.1	27.0
E-Aug-BS	300	10.0	1.0	9.0	27.0	2.5	0.0	500.0	0.23	27.0
Pump+	300	0.0	0.0	6.0	25.0	3.8	0.08	500.0	0.1	0.0
Pump−	300	0.0	0.0	6.0	25.0	3.8	0.08	500.0	0.1	0.0
Phrenic (Phr)	300	10.0	1.0	6.0	25.0	3.8	0.08	500.0	0.1	7.0
Exp Motor	300	10.0	1.0	9.0	27.0	2.5	0.0	500.0	0.023	0.0

Parameter values for initial model network populations. Variable names used by MacGregor (1987) are in italics. All values representing voltages are relative to the resting potential, which is considered equal to zero. *N* is the number of neurons simulated in each population. *THO,* the resting threshold, is normally distributed in the population around the value of THO with a standard deviation equal to the "THO variability" value. *TMEM* is the membrane time constant. *B* is the amplitude of the post-spike increase in potassium conductance. *TGK* is the time constant of the potassium conductance decay following an action potential. *C* and *TTH* define the change in threshold associated with spike adaptation. *C* is the ratio of the threshold increase to the membrane potential increase; its value is between 0 and 1. *TTH* is the time constant of the rise in threshold with spike adaptation. *Noise Amplitude.* Each cell has an internal noise generator that acts like two synapses, one with an equilibrium potential of 70 mV above resting and the other with −70 mV. Each acts like it has an incoming firing probability of 0.05 per time step, and a synapse time constant of 1.5 ms. This parameter is the conductance that gets added to the synapse conductance on each (virtual) spike. *DC.* An injected current will raise the membrane potential by an amount that is inversely proportional to the membrane conductance. Instead of being specified directly as a current, this parameter is specified in mV, and it is interpreted as the current that is required to raise the membrane potential by the specified number of mV when the membrane conductance has its resting value. The effect on the membrane potential at other membrane conductances will be inversely proportional to the conductance. Note also that as in other types of IF neuron models, our neuron models do not actually generate action potential-like spikes but only identified moments of spikes, so "spiking" shown in all neuron simulations are represented graphically by assigning vertical spike-like lines at computed times of threshold crossing.

TABLE A2. *I-Driver neuron parameters*

I-Driver Parameter	Value
Time constant for h	2000 ms
Half-voltage for h	−51 mV
NaP conductance	3.0 nS
Slope for h	5.0 mV
Half-voltage for activation	−43.0 mV
Slope for activation	−6.0 mV
Reset voltage @ $h = 0$	−42.0 mV
Threshold voltage	−37.0 mV
Applied current (I_{app})	0.0 pA
Noise amplitude	0.1 nS

The I-Driver neuron was modeled using "hybrid IF conditional burster model" derived from Breen et al. (2003). All parameters in this model correspond to Breen et al. model; h is inactivation variable of the persistent sodium (NaP) channel The following modifications of the original Breen et al. model were made: the *Threshold voltage* parameter was set constant (not dependent on h) and reset of h with each spike $\Delta h\ (h) = -0.00185h$.

TABLE A3. *Simulated PSR population parameters for model networks*

	Value	
PSR Population Parameter	Model 1	Model 2
Rise time constant, ms	500.0	500.0
Fall time constant, ms	500.0	100.0

Lung volume dynamics were not directly simulated in our models. Input to the pulmonary stretch receptor (PSR) population was formed via low-pass filtering of the output of the Phr (Fig. 1) population or I-Aug-BS/Phr population (Fig. 4) with rise and fall time constants given in the table.

TABLE A4. *Connectivity for the initial model represented in Fig. 1*

Source Population	Target Population	Synaptic Type	Minimum Conduction Time	Maximum Conduction Time	No. of Terminals	Synaptic Strength	Source Population *N*	Target Population *N*	Divergence	Mean No. of Terminals	Convergence
I-Driver	I-Dec	Ex	0	4	100	0.006	300	300	84.99 ± 3.14	1.18	84.99 ± 7.54
I-Driver	I-Aug-BS	Ex	0	5	100	0.005	300	300	84.98 ± 3.14	1.18	84.98 ± 7.44
I-Driver	I-Driver	Ex	0	4	50	0.003	300	300	46.34 ± 1.76	1.08	46.34 ± 5.84
E-Dec-P	I-Driver	Inh_2	0	5	100	0.012	300	300	85.20 ± 3.05	1.17	85.20 ± 9.59
E-Dec-P	E-Aug-early	Inh_1	0	2	150	0.006	300	300	118.24 ± 4.01	1.27	118.24 ± 8.86
E-Dec-P	E-Aug-late	Inh_1	2	4	150	0.02	300	300	118.10 ± 3.94	1.27	118.10 ± 9.61
E-Dec-P	VRC IE	Inh_1	0	2	24	0.2	300	99	21.36 ± 1.41	1.12	64.74 ± 5.23
E-Dec-P	I-Dec	Inh_1	0	0	100	0.2	300	300	85.07 ± 3.10	1.18	85.07 ± 7.21
E-Dec-P	PRG I	Inh_2	0	1	100	0.001	300	100	63.24 ± 3.09	1.58	189.71 ± 8.08
E-Dec-P	I-Aug-BS	Inh_1	0	2	50	0.1	300	300	46.19 ± 1.72	1.08	46.19 ± 5.43
E-Dec-P	E-Aug-BS	Inh_1	0	5	125	0.015	300	300	102.22 ± 3.56	1.22	102.22 ± 9.65
I-Dec	E-Aug-early	Inh_1	0	2	115	1.25	300	300	95.67 ± 3.39	1.20	95.67 ± 7.14
I-Dec	E-Dec-P	Inh_1	0	5	115	0.3	300	300	95.60 ± 3.52	1.20	95.60 ± 7.69
I-Dec	I-Aug-BS	Inh_2	0	1	210	0.006	300	300	151.59 ± 5.04	1.39	151.59 ± 8.80
I-Dec	E-Aug-late	Inh_2	0	5	115	1.0	300	300	95.71 ± 3.51	1.20	95.71 ± 7.84
I-Dec	VRC IE	Inh_1	0	4	100	0.029	300	99	63.21 ± 3.10	1.58	191.54 ± 7.38
I-Dec	E-Dec-T	Inh_1	0	5	100	0.015	300	300	84.90 ± 2.96	1.18	84.90 ± 9.43
I-Dec	E-Aug-BS	Inh_1	0	5	125	0.045	300	300	102.22 ± 3.56	1.22	102.22 ± 9.65
I-Dec	PRG EI	Ex	0	1	100	0.0005	300	100	63.47 ± 3.07	1.58	190.42 ± 9.05
I-Aug-BS	I-Aug-BS	Ex	0	5	50	0.02	300	300	45.99 ± 1.77	1.09	45.99 ± 5.31
I-Aug-BS	PRG I	Ex	0	1	100	0.002	300	100	63.43 ± 3.01	1.58	190.28 ± 11.40
I-Aug-BS	Phrenic	Ex	0	3	50	0.02	300	300	46.35 ± 1.71	1.08	46.35 ± 6.00
I-Aug-BS	VRC IE	Ex	0	5	50	0.004	300	99	39.38 ± 2.42	1.27	119.34 ± 6.86
E-Aug-early	E-Dec-P	Inh_1	0	2	110	0.014	300	300	91.85 ± 3.43	1.20	91.85 ± 8.07
E-Aug-early	I-Dec	Inh_1	0	5	100	0.05	300	300	85.13 ± 2.98	1.17	85.13 ± 7.70
E-Aug-early	I-Aug-BS	Inh_1	0	2	150	0.06	300	300	118.48 ± 4.08	1.27	118.48 ± 8.37
E-Aug-early	VRC IE	Inh_1	0	2	24	0.02	300	99	21.46 ± 1.29	1.12	65.02 ± 6.96
E-Aug-early	Phrenic	Inh_1	0	2	150	0.1	300	300	118.31 ± 4.21	1.27	118.31 ± 7.57
E-Aug-early	E-Dec-T	Inh_1	0	2	100	0.006	300	300	85.13 ± 2.94	1.17	85.13 ± 9.11
E-Aug-early	E-Aug-late	Inh_1	0	2	50	0.001	300	300	46.01 ± 1.81	1.09	46.01 ± 6.57
E-Aug-late	E-Aug-early	Inh_1	0	2	50	0.004	300	300	46.23 ± 1.78	1.08	46.23 ± 9.43
E-Aug-late	I-Dec	Inh_1	0	4	55	0.01	300	300	50.33 ± 1.87	1.09	50.33 ± 6.68
E-Aug-late	I-Aug-BS	Inh_1	0	2	150	0.06	300	300	118.09 ± 3.79	1.27	118.09 ± 7.65
E-Aug-late	E-Dec-P	Inh_1	0	2	115	0.014	300	300	95.57 ± 3.26	1.20	95.57 ± 9.85
E-Aug-late	Phrenic	Inh_1	0	2	150	0.12	300	300	118.14 ± 4.18	1.27	118.14 ± 8.44
E-Aug-late	VRC IE	Inh_1	0	2	24	0.02	300	99	21.32 ± 1.39	1.13	64.62 ± 7.03
E-Aug-late	E-Dec-T	Inh_1	0	2	100	0.015	300	300	85.18 ± 3.01	1.17	85.18 ± 6.53
E-Aug-late	E-Aug-BS	Inh_1	0	5	100	0.01	300	300	85.20 ± 3.05	1.17	85.20 ± 9.59
E-Aug-late	PRG E	Ex	0	1	100	0.005	300	100	63.34 ± 3.11	1.58	190.03 ± 8.09
VRC IE	I-Dec	Inh_2	0	4	200	0.05	99	300	146.65 ± 4.99	1.36	48.39 ± 5.40
VRC IE	I-Aug-BS	Inh_2	0	5	200	0.02	99	300	146.07 ± 4.45	1.37	48.20 ± 4.92
VRC IE	E-Aug-BS	Inh_1	0	5	100	0.03	99	300	84.91 ± 3.06	1.18	28.02 ± 4.41
Phrenic	PSR	Ex	0	3	50	0.03	300	300	45.92 ± 1.84	1.09	45.92 ± 6.62
VRC NRM	PRG cIE	Inh_1	0	2	100	0.001	300	100	63.28 ± 3.18	1.58	189.84 ± 7.52
VRC NRM	PRG I	Ex	0	1	100	0.002	300	100	63.25 ± 3.00	1.58	189.74 ± 8.31
VRC NRM	PRG rIE	Inh_2	0	1	100	0.002	300	100	63.41 ± 3.22	1.58	190.23 ± 7.92
PRG cIE	I-Driver	Ex	0	5	100	0.03	100	300	85.68 ± 2.78	1.17	28.56 ± 4.45
PSR	Pump+	Ex	0	3	50	0.015	300	300	46.11 ± 1.76	1.08	46.11 ± 6.15
PSR	Pump−	Ex	0	3	50	0.015	300	300	46.23 ± 1.78	1.08	46.23 ± 9.43
PRG EI	PRG cIE	Inh_1	0	1	100	0.05	100	100	63.17 ± 2.78	1.58	63.17 ± 5.11
PRG EI	E-Dec-T	Ex	0	5	100	0.04	100	300	85.12 ± 2.95	1.17	28.37 ± 4.38
PRG EI	VRC IE	Ex	0	1	50	0.001	100	99	39.21 ± 2.16	1.28	39.61 ± 3.92
PRG E	PRG EI	Ex	0	1	100	0.008	100	100	63.09 ± 2.87	1.59	63.09 ± 4.46
PRG E	I-Dec	Inh_1	0	1	100	0.005	100	300	84.70 ± 3.14	1.18	28.23 ± 4.52
PRG E	PRG rIE	Inh_1	0	1	100	0.011	100	100	62.86 ± 3.19	1.59	62.86 ± 5.92
PRG rIE	E-Dec-P	Ex	0	5	100	0.025	100	300	85.48 ± 2.95	1.17	28.49 ± 4.34
PRG rIE	VRC IE	Ex	0	1	100	0.001	100	99	63.13 ± 3.05	1.58	63.77 ± 5.20
Pump−	PRG E	Pre	0	1	100	0.95	300	100	63.46 ± 3.14	1.58	190.39 ± 7.82
Pump−	I-Dec	Inh_1	0	2	25	0.0035	300	300	23.98 ± 0.90	1.04	23.98 ± 5.97
Pump−	PRG I	Pre	0	1	100	0.95	300	100	63.14 ± 3.05	1.58	189.43 ± 8.77
Pump−	PRG I	Pre	0	1	100	0.95	300	100	63.12 ± 3.16	1.58	189.37 ± 8.97
Pump−	PRG rIE	Pre	0	1	100	0.95	300	100	63.37 ± 3.06	1.58	190.12 ± 9.62
Pump−	PRG rIE	Pre	0	1	100	0.95	300	100	63.43 ± 3.01	1.58	190.28 ± 11.40
Pump+	E-Dec-P	Ex	0	2	100	0.002	300	300	85.47 ± 2.95	1.17	85.47 ± 8.14
Pump+	VRC IE	Ex	0	2	25	0.004	300	99	22.17 ± 1.41	1.13	67.17 ± 17.13
Pump+	I-Aug-BS	Ex	0	2	25	0.002	300	300	24.07 ± 0.91	1.04	24.07 ± 4.15
Pump+	E-Dec-T	Ex	0	2	100	0.002	300	300	85.12 ± 3.16	1.17	85.12 ± 6.94

TABLE A4. *(continued)*

Source Population	Target Population	Synaptic Type	Minimum Conduction Time	Maximum Conduction Time	No. of Terminals	Synaptic Strength	Source Population *N*	Target Population *N*	Divergence	Mean No. of Terminals	Convergence
E-Aug-BS	Exp Motor	Ex	0	5	200	0.01	300	300	146.21 ± 4.65	1.37	146.21 ± 9.31
PRG E-Other	PRG cIE	Inh_1	0	1	100	0.001	100	100	63.91 ± 3.34	1.56	63.91 ± 4.69
PRG I	PRG E-Other	Inh_1	0	1	100	0.05	100	100	63.91 ± 3.34	1.56	63.91 ± 4.69
PRG I	PRG rIE	Inh_1	0	1	100	0.02	100	100	62.86 ± 3.19	1.59	62.86 ± 5.92
PRG I	I-Aug-BS	Ex	0	4	50	0.005	100	300	46.36 ± 1.83	1.08	15.45 ± 3.58
PRG I	VRC IE	Ex	0	5	50	0.007	100	99	39.58 ± 2.66	1.26	39.98 ± 6.47
PRG NRM+	E-Dec-P	Ex	0	1	100	0.01	100	300	84.98 ± 3.08	1.18	28.33 ± 4.71
PRG NRM+	E-Dec-T	Ex	0	1	100	0.01	100	300	84.86 ± 2.53	1.18	28.29 ± 4.38
PRG NRM+	I-Aug-BS	Ex	0	1	100	0.01	100	300	84.79 ± 2.94	1.18	28.26 ± 4.55
PRG NRM+	VRC IE	Ex	0	1	100	0.01	100	99	63.07 ± 3.05	1.59	63.71 ± 4.82
PRG NRM+	I-Driver	Ex	0	5	100	0.11	100	300	84.79 ± 2.94	1.18	28.26 ± 4.55
PRG NRM+	E-Aug-late	Ex	0	4	50	0.003	100	300	46.36 ± 1.83	1.08	15.45 ± 3.58
PRG NRM+	E-Aug-early	Ex	0	4	50	0.003	100	300	46.36 ± 1.83	1.08	15.45 ± 3.58
PRG NRM+	PRG rIE	Ex	0	1	100	0.015	100	100	62.86 ± 3.19	1.59	62.86 ± 5.92
PRG NRM−	VRC NRM	Inh_1	0	1	100	0.001	100	300	84.68 ± 2.67	1.18	28.23 ± 4.60

Connections between individual neurons were made according to a sequence of pseudorandom numbers calculated from a unique seed number for each source-to-target connection. Targets were chosen with replacement. This table includes the means ± SD of the number of neurons in each target population innervated by each source neuron in each population. Corresponding values are also shown for source neurons that innervated each target neuron in each population. These data indicate the extent of divergence and convergence, respectively. Most neurons in each source population made a single terminal connection with each target neuron. Mean No. of Terminals, the mean number of terminals from each source neuron innervating each target neuron. The efficacy of connections between populations of neurons was influenced by the change in conductance associated with each action potential at a synapse (Synaptic Strength) and the number of terminals for each axon. Synaptic types were distinguished by their equilibrium potentials and time constants. The time constant of some synapses was slightly longer than others because troughs in cross-correlograms from which the particular synaptic connections were inferred tended to have longer durations. Four types of synapses were used in the first series of simulations: excitatory (Ex, equilibrium potential of 115.0 mV; time constant, 1.5 ms); type 1 inhibitory (Inh_1, equilibrium potential, − 25.0 mV; time constant, 1.5 ms); type 2 inhibitory (Inh_2, equilibrium potential, −25.0 mV; time constant, 2.0 ms); pre-synaptic modulation (Pre, time constant, 1.5 ms). If the value of the pre-synaptic modulatory strength parameter (Synaptic Strength) was <1.0, the strength of the connection it modulates was reduced to the product of the presynaptic Synaptic Strength parameter and target synapse conductance. If the presynaptic Synaptic Strength parameter was >1.0, the amount by which it was greater than 1 is added to its target synapse's conductance. Minimum and maximum conduction times, are expressed in 0.5-ms simulation clock ticks for each source-to-target axon population. No. of Terminals, number of terminals from source neuron.

TABLE A5. *Population parameters for model represented in Fig. 4*

Population Variables	Size *N*	Resting Threshold, mV *THO*	THO Variability, mV	Membrane Time Constant *TMEM*	Post-spike Increase in G_K^+ *B*	Post-spike G_K^+ Time Constant, ms *TGK*	Adaptation Threshold Increase C	Adaptation, ms *TTH*	Noise Amp.	DC, mV
PRG I	100	10.0	1.0	9.0	20.0	7.0	0.0	500.0	0.03	2.0
PRG rIE	100	10.0	1.0	9.0	20.0	7.0	0.0	500.0	0.3	5.0
PRG cIE	100	10.0	1.0	9.0	20.0	7.0	0.0	500.0	0.3	5.0
PRG E	100	10.0	1.0	9.0	20.0	7.0	0.0	500.0	0.3	13.0
PRG EI	100	10.0	1.0	9.0	20.0	7.0	0.0	500.0	0.3	20.0
PRG NRM	100	10.0	1.0	9.0	20.0	7.0	0.0	500.0	0.03	25.0
VRC NRM	300	10.0	1.0	9.0	20.0	7.0	0.0	500.0	0.03	25.0
I-DRIVER	300					See Table A2				
I-Dec	300	10.0	1.0	6.0	25.5	6.63	0.5	500.0	0.3	32.0
I-Aug	300	10.0	1.0	6.0	25.0	3.8	0.0	5000.0	0.5	8.0
VRC IE	99	10.0	1.0	9.0	5.6	5.0	0.0	1000.0	0.05	12.0
E-Dec-P	300	8.0	1.0	9.0	27.0	2.5	0.8	1000.0	0.1	9.0
E-Dec-T	300	8.0	1.0	9.0	27.0	2.5	0.8	2000.0	0.3	0.0
E-Aug-early	300	10.0	1.0	6.0	27.0	2.5	0.0	500.0	0.3	30.0
E-Aug-late	300	10.0	1.0	9.0	27.0	2.5	0.0	500.0	0.1	27.0
E-Aug-late-HT	300	10.0	1.0	9.0	27.0	2.5	0.0	500.0	0.3	0.0
E-Aug-BS	300	10.0	1.0	6.0	25.0	3.8	0.08	500.0	0.3	5.0
Pump+	300	0.0	0.0	6.0	25.0	3.8	0.08	500.0	0.1	0.0
Pump−	300	0.0	0.0	6.0	25.0	3.8	0.08	500.0	0.1	0.0
I-Aug-BS/PHR	300	10.0	1.0	6.0	25.0	3.8	0.08	500.0	0.3	5.0
Lum (Exp MN)	300	10.0	1.0	6.0	25.0	3.8	0.08	500.0	0.3	5.0
ILM	100	10.0	1.0	6.0	25.0	3.8	0.08	500.0	0.1	0.0
ELM	100	10.0	1.0	6.0	25.0	3.8	0.08	500.0	0.1	0.0
Hypoxia	100	10.0	1.0	9.0	20.0	7.0	0.0	500.0	0.1	0.0
Second-order (cough)	100	10.0	1.0	9.0	20.0	7.0	0.3	500.0	0.1	0.0

TABLE A6. *Connectivity for the model represented in Fig. 4*

Source Population	Target Population	Synaptic Type	Minimum Conduction Time	Maximum Conduction Time	No. of Terminals	Synaptic Strength	Source Population *N*	Target Population *N*	Divergence	Mean No. of Terminals	Convergence
I-Driver	I-Dec	Ex	0	4	100	0.006	300	300	84.99 ± 3.14	1.18	84.99 ± 7.54
I-Driver	I-Aug	Ex	0	5	100	0.005	300	300	84.98 ± 3.14	1.18	84.98 ± 7.44
I-Driver	I-Driver	Ex	0	4	50	0.003	300	300	46.34 ± 1.76	1.08	46.34 ± 5.84
E-Dec-P	I-Driver	Inh_2	0	5	100	0.015	300	300	85.20 ± 3.05	1.17	85.20 ± 9.59
E-Dec-P	E-Aug-early	Inh_1	0	2	150	0.012	300	300	118.24 ± 4.01	1.27	118.24 ± 8.86
E-Dec-P	E-Aug-late	Inh_1	2	4	150	0.02	300	300	118.10 ± 3.94	1.27	118.10 ± 9.61
E-Dec-P	VRC IE	Inh_1	0	2	50	0.1	300	99	39.33 ± 2.31	1.27	119.18 ± 7.22
E-Dec-P	I-Dec	Inh_1	0	2	200	0.2	300	300	146.07 ± 4.42	1.37	146.07 ± 8.71
E-Dec-P	E-Aug-BS	Inh_1	0	4	100	0.01	300	300	85.51 ± 3.01	1.17	85.51 ± 7.16
E-Dec-P	I-Aug	Inh_1	0	2	50	0.1	300	300	46.19 ± 1.72	1.08	46.19 ± 5.43
E-Dec-P	PRG rIE	Ex	2	4	100	0.001	300	100	63.13 ± 2.98	1.58	189.39 ± 6.74
E-Dec-P	PRG cIE	Ex	2	4	100	0.001	300	100	63.23 ± 3.19	1.58	189.70 ± 9.56
E-Dec-P	ELM	Ex	2	4	150	0.004	300	300	118.10 ± 3.94	1.27	118.10 ± 9.61
I-Dec	E-Aug-early	Inh_1	0	2	115	1.0	300	300	95.67 ± 3.39	1.20	95.67 ± 7.14
I-Dec	E-Dec-P	Inh_1	0	5	200	0.2	300	300	145.80 ± 5.20	1.37	145.80 ± 9.31
I-Dec	I-Aug	Inh_2	0	1	200	0.008	300	300	146.63 ± 4.89	1.36	146.63 ± 8.54
I-Dec	E-Aug-late	Inh_2	0	5	115	1.0	300	300	95.71 ± 3.51	1.20	95.71 ± 7.84
I-Dec	VRC IE	Inh_1	0	4	100	0.029	300	99	63.21 ± 3.10	1.58	191.54 ± 7.38
I-Dec	E-Dec-T	Inh_1	0	5	100	0.05	300	300	84.90 ± 2.96	1.18	84.90 ± 9.43
I-Dec	ILM	Ex	0	3	50	0.004	300	300	46.35 ± 1.71	1.08	46.35 ± 6.00
I-Dec	E-Aug-BS	Inh_1	0	4	100	0.02	300	300	85.44 ± 3.02	1.17	85.44 ± 9.96
I-Dec	PRG EI	Ex	2	4	100	0.001	300	100	63.33 ± 3.16	1.58	190.00 ± 8.78
I-Dec	PRG I	Ex	2	4	100	0.0005	300	100	63.50 ± 3.23	1.57	190.51 ± 8.03
I-Dec	PRG I	Inh_2	2	4	100	0.0005	300	100	63.66 ± 3.21	1.57	190.98 ± 8.42
I-Dec	PRG rIE	Inh_1	2	4	100	0.0001	300	100	63.55 ± 3.04	1.57	190.65 ± 8.05
I-Dec	PRG cIE	Inh_2	2	4	100	0.0001	300	100	63.27 ± 3.06	1.58	189.80 ± 8.43
I-Aug	I-Aug	Ex	0	5	50	0.02	300	300	45.99 ± 1.77	1.09	45.99 ± 5.31
I-Aug	PRG cIE	Inh_2	2	4	100	0.0001	300	100	63.43 ± 3.19	1.58	190.28 ± 9.05
I-Aug	I-Aug-BS/PHR	Ex	0	3	100	0.03	300	300	85.20 ± 3.01	1.17	85.20 ± 7.27
I-Aug	ILM	Ex	0	3	50	0.03	300	300	46.35 ± 1.71	1.08	46.35 ± 6.00
I-Aug	VRC IE	Ex	0	5	100	0.003	300	99	63.05 ± 3.25	1.59	191.06 ± 7.37
I-Aug	PRG I	Ex	2	4	100	0.0025	300	100	63.59 ± 2.94	1.57	190.76 ± 7.71
I-Aug	PRG rIE	Inh_1	2	4	100	0.0001	300	100	63.43 ± 2.95	1.58	190.29 ± 8.57
I-Aug	E-Aug-BS	Inh_1	0	4	1000	0.1	300	300	289.42 ± 2.98	3.46	289.42 ± 2.86
E-Aug-early	E-Dec-P	Inh_1	0	2	110	0.014	300	300	91.85 ± 3.43	1.20	91.85 ± 8.07
E-Aug-early	I-Dec	Inh_1	0	5	100	0.06	300	300	85.13 ± 2.98	1.17	85.13 ± 7.70
E-Aug-early	I-Aug	Inh_1	0	2	150	0.06	300	300	118.48 ± 4.08	1.27	118.48 ± 8.37
E-Aug-early	VRC IE	Inh_1	0	2	24	0.05	300	99	21.46 ± 1.29	1.12	65.02 ± 6.96
E-Aug-early	I-Aug-BS/PHR	Inh_1	0	2	150	0.001	300	300	118.31 ± 4.21	1.27	118.31 ± 7.57
E-Aug-early	E-Dec-T	Inh_1	0	2	100	0.05	300	300	85.13 ± 2.94	1.17	85.13 ± 9.11
E-Aug-early	E-Aug-late	Inh_1	0	2	50	0.001	300	300	46.01 ± 1.81	1.09	46.01 ± 6.57
E-Aug-early	PRG E	Ex	2	4	100	0.002	300	100	63.08 ± 2.85	1.59	189.25 ± 7.68
E-Aug-early	E-Aug-BS	Ex	0	3	50	0.02	300	300	46.35 ± 1.71	1.08	46.35 ± 6.00
E-Aug-early	PRG I	Inh_2	2	4	100	0.0005	300	100	63.08 ± 2.85	1.59	189.25 ± 7.68
E-Aug-late	E-Aug-early	Inh_1	0	2	200	0.04	300	300	145.91 ± 4.71	1.37	145.91 ± 9.07
E-Aug-late	I-Dec	Inh_1	0	4	55	0.01	300	300	50.33 ± 1.87	1.09	50.33 ± 6.68
E-Aug-late	I-Aug	Inh_1	0	2	150	0.06	300	300	118.09 ± 3.79	1.27	118.09 ± 7.65
E-Aug-late	E-Dec-P	Inh_1	0	2	115	0.014	300	300	95.57 ± 3.26	1.20	95.57 ± 9.85
E-Aug-late	I-Aug-BS/PHR	Inh_1	0	2	150	0.002	300	300	118.14 ± 4.18	1.27	118.14 ± 8.44
E-Aug-late	VRC IE	Inh_1	0	2	24	0.02	300	99	21.32 ± 1.39	1.13	64.62 ± 7.03
E-Aug-late	E-Dec-T	Inh_1	0	2	100	0.05	300	300	85.18 ± 3.01	1.17	85.18 ± 6.53
E-Aug-late	E-Aug-BS	Inh_1	0	4	100	0.015	300	300	85.16 ± 3.38	1.17	85.16 ± 10.32
E-Aug-late	E-Aug-late-HT	Ex	0	3	50	0.01	300	300	45.99 ± 1.70	1.09	45.99 ± 6.08
E-Aug-late	ELM	Inh_1	2	4	500	0.15	300	300	243.18 ± 5.04	2.06	243.18 ± 7.13
VRC IE	I-Dec	Inh_2	0	4	200	0.05	99	300	146.65 ± 4.99	1.36	48.39 ± 5.40
VRC IE	I-Aug	Inh_2	0	5	200	0.02	99	300	146.07 ± 4.45	1.37	48.20 ± 4.92
I-Aug-BS/PHR	PSR	Ex	0	3	100	0.016	300	300	84.91 ± 3.04	1.18	84.91 ± 8.03
VRC NRM	PRG rIE	Inh_2	0	1	100	0.002	300	100	63.41 ± 3.22	1.58	190.23 ± 7.92
VRC NRM	PRG cIE	Inh_2	0	1	100	0.002	300	100	63.37 ± 3.02	1.58	190.12 ± 7.75
VRC NRM	PRG I	Ex	0	1	100	0.002	300	100	63.25 ± 3.00	1.58	189.74 ± 8.31
E-Aug-late-HT	E-Aug-BS	Inh_1	0	3	600	0.1	300	300	259.67 ± 4.67	2.31	259.67 ± 5.85

TABLE A6. *(continued)*

Source Population	Target Population	Synaptic Type	Minimum Conduction Time	Maximum Conduction Time	No. of Terminals	Synaptic Strength	Source Population *N*	Target Population *N*	Divergence	Mean No. of Terminals	Convergence
PSR	Pump+	Ex	0	3	50	0.015	300	300	46.11 ± 1.76	1.08	46.11 ± 6.15
PSR	Pump−	Ex	0	3	50	0.015	300	300	46.23 ± 1.78	1.08	46.23 ± 9.43
PRG cIE	I-Driver	Ex	0	5	100	0.001	100	300	85.68 ± 2.78	1.17	28.56 ± 4.45
Pump−	PRG E	Pre	0	4	100	0.99	300	100	63.19 ± 2.88	1.58	189.58 ± 7.28
Pump−	I-Dec	Inh_1	0	2	25	0.0035	300	300	23.98 ± 0.90	1.04	23.98 ± 5.97
Pump−	PRG I	Pre	0	4	100	0.99	300	100	63.53 ± 2.94	1.57	190.58 ± 7.02
Pump−	PRG EI	Pre	2	4	100	0.99	300	100	63.55 ± 2.95	1.57	190.64 ± 7.44
Pump−	PRG rIE	Pre	0	4	100	0.99	300	100	63.63 ± 3.02	1.57	190.88 ± 9.09
Pump−	PRG cIE	Pre	0	4	100	0.99	300	100	63.63 ± 3.02	1.57	190.88 ± 9.09
Pump+	E-Dec-P	Ex	0	2	100	0.01	300	300	85.47 ± 2.95	1.17	85.47 ± 8.14
Pump+	VRC IE	Ex	0	2	100	0.004	300	99	63.10 ± 2.99	1.58	191.20 ± 11.20
Pump+	I-Aug	Ex	0	2	25	0.002	300	300	24.07 ± 0.91	1.04	24.07 ± 4.15
Pump+	E-Dec-T	Ex	0	2	100	0.002	300	300	85.12 ± 3.16	1.17	85.12 ± 6.94
Pump+	E-Aug-BS	Ex	0	4	100	0.008	300	300	85.19 ± 3.15	1.17	85.19 ± 7.24
E-Dec-T	I-Aug-BS/PHR	Inh_1	0	4	100	0.05	300	300	84.99 ± 3.14	1.18	84.99 ± 7.54
E-Dec-T	PRG rIE	Ex	2	4	100	0.001	300	100	63.26 ± 3.11	1.58	189.77 ± 11.78
E-Dec-T	PRG I	Ex	2	4	100	0.0005	300	100	63.33 ± 3.02	1.58	189.98 ± 9.72
E-Dec-T	PRG I	Inh_2	2	4	100	0.0005	300	100	63.20 ± 3.13	1.58	189.60 ± 7.79
E-Dec-T	PRG rIE	Inh_1	2	4	100	0.0005	300	100	63.57 ± 3.16	1.57	190.70 ± 7.57
E-Dec-T	PRG cIE	Ex	2	4	100	0.001	300	100	63.20 ± 3.18	1.58	189.61 ± 7.72
E-Dec-T	PRG cIE	Inh_2	2	4	100	0.0005	300	100	63.40 ± 3.17	1.58	190.20 ± 9.74
PRG rIE	PRG EI	Inh_1	2	4	100	0.03	100	100	63.79 ± 3.24	1.57	63.79 ± 4.98
PRG rIE	VRC IE	Ex	0	1	100	0.001	100	99	62.90 ± 3.28	1.59	63.54 ± 4.65
PRG rIE	E-Dec-P	Ex	0	5	100	0.02	100	300	85.06 ± 2.76	1.18	28.35 ± 4.15
PRG EI	PRG rIE	Ex	2	4	100	0.002	100	100	63.47 ± 3.20	1.58	63.47 ± 4.78
PRG EI	PRG cIE	Ex	2	4	100	0.002	100	100	63.36 ± 3.47	1.58	63.36 ± 4.41
PRG EI	VRC IE	Ex	0	4	50	0.0003	100	99	39.46 ± 2.35	1.27	39.86 ± 5.11
PRG EI	E-Dec-T	Ex	0	4	100	0.01	100	300	85.16 ± 3.33	1.17	28.39 ± 5.10
PRG E	PRG rIE	Inh_1	2	4	100	0.0001	100	100	63.17 ± 3.15	1.58	63.17 ± 5.22
PRG E	PRG cIE	Inh_1	2	4	100	0.0001	100	100	63.47 ± 3.13	1.58	63.47 ± 5.60
PRG E	I-Dec	Inh_1	0	1	100	0.008	100	300	85.14 ± 3.03	1.17	28.38 ± 4.11
PRG NRM	PRG I	Ex	0	4	100	0.015	100	100	63.26 ± 3.28	1.58	63.26 ± 4.40
PRG NRM	PRG I	Inh_1	0	4	100	0.05	100	100	63.62 ± 3.11	1.57	63.62 ± 4.61
PRG NRM	I-Driver	Ex	0	5	100	0.12	100	300	85.10 ± 3.00	1.18	28.37 ± 4.51
PRG NRM	VRC IE	Ex	0	1	100	0.01	100	99	63.02 ± 2.53	1.59	63.66 ± 4.67
PRG NRM	I-Aug	Ex	0	1	100	0.01	100	300	85.21 ± 2.94	1.17	28.40 ± 4.81
PRG NRM	E-Aug-early	Ex	0	4	100	0.025	100	300	85.82 ± 3.10	1.17	28.61 ± 4.20
PRG NRM	E-Aug-late	Ex	0	4	50	0.003	100	300	45.82 ± 1.89	1.09	15.27 ± 3.67
PRG NRM	E-Dec-P	Ex	0	1	100	0.01	100	300	84.87 ± 3.22	1.18	28.29 ± 4.18
PRG NRM	E-Dec-T	Ex	0	1	100	0.1	100	300	85.35 ± 3.04	1.17	28.45 ± 4.06
PRG NRM	VRC NRM	Inh_1	0	1	100	0.001	100	300	85.11 ± 2.96	1.17	28.37 ± 5.07
E-Aug-BS	Lum (Exp MN)	Ex	0	4	100	0.003	300	300	85.19 ± 3.15	1.17	85.19 ± 7.24
PRG I	PRG rIE	Ex	0	4	100	0.005	100	100	62.93 ± 2.89	1.59	62.93 ± 5.56
PRG I	VRC IE	Ex	0	5	100	0.005	100	99	63.61 ± 3.41	1.57	64.25 ± 4.84
PRG I	I-Aug	Ex	0	4	50	0.005	100	300	46.17 ± 1.67	1.08	15.39 ± 3.39
PRG I	PRG cIE	Ex	0	4	100	0.005	100	100	63.67 ± 2.85	1.57	63.67 ± 4.57

TABLE A7. *Parameters for neuron populations relaying perturbations of the extended network model*

Population	Size	Resting Threshold, mV	THO Variability, mV	Membrane Time Constant	Post-spike Increase in G_K^+	Post-spike G_K^+ Time Constant, ms	Adaptation Threshold Increase	Adaptation, ms	Noise Amplitude	DC, mV
Variables	*N*	*THO*		*TMEM*	*B*	*TGK*	*C*	*TTH*		
Second-order (cough)	100	10.0	1.0	9.0	20.0	7.0	0.3	500.0	0.1	0.0
Hypoxia effect	100	10.0	0.0	9.0	20.0	7.0	0.0	500.0	0.1	0.0
Biasing population*	100	10.0	1.0	9.0	20.0	7.0	0.0	500.0	0.03	25.0

*The biasing population excited I-Aug neurons during the state represented in Fig. 10*A, right.* See text for further details.

TABLE A8. *Connectivity matrix for neuron populations relaying perturbations of the extended network model*

Source Population	Target Population	Synaptic Type	Minimum Conduction Time	Maximum Conduction Time	No. of Terminals	Synaptic Strength	Source Population *N*	Target Population *N*	Divergence	Mean No. of Terminals	Convergence
Second-order (cough)	I-Dec	Ex	0	3	100	0.038	100	300	85.25 ± 2.83	1.17	28.42 ± 5.15
Second-order (cough)	I-Aug	Ex	0	3	100	0.02	100	300	85.25 ± 2.83	1.17	28.42 ± 5.15
Second-order (cough)	E-Dec-P	Ex	0	3	100	0.015	100	300	85.25 ± 2.83	1.17	28.42 ± 5.15
Second-order (cough)	E-Aug-early	Ex	0	3	100	0.1	100	300	85.25 ± 2.83	1.17	28.42 ± 5.15
Second-order (cough)	E-Aug-late	Ex	0	3	100	0.06	100	300	85.25 ± 2.83	1.17	28.42 ± 5.15
Second-order (cough)	E-Aug-BS	Ex	0	4	100	0.001	100	300	85.76 ± 2.62	1.17	28.59 ± 4.46
Second-order (cough)	Pump-	Inh_1	0	4	250	0.4	100	300	170.45 ± 4.98	1.47	56.82 ± 4.58
Second-order (cough)	VRC IE	Inh_1	0	3	100	0.2	100	99	63.13 ± 3.05	1.58	63.77 ± 5.20
Second-order (cough)	PRG cIE	Ex	0	3	100	0.001	100	100	63.59 ± 3.21	1.57	63.59 ± 5.84
Second-order (cough)	PRG rIE	Ex	0	3	100	0.001	100	100	63.59 ± 3.21	1.57	63.59 ± 5.84
Second-order (cough)	PRG I	Ex	0	3	100	0.001	100	100	63.59 ± 3.21	1.57	63.59 ± 5.84
Second-order (cough)	PRG E	Ex	0	3	100	0.001	100	100	63.59 ± 3.21	1.57	63.59 ± 5.84
Second-order (cough)	PRG EI	Ex	0	3	100	0.001	100	100	63.59 ± 3.21	1.57	63.59 ± 5.84
Second-order (cough)	Lumbar	Pre	0	4	100	1.3	100	300	85.05 ± 3.08	1.18	28.35 ± 4.39
Hypoxia effect	VRC IE	Ex	0	3	100	0.001	100	99	62.50 ± 3.22	1.60	63.13 ± 5.42
Hypoxia effect	I-Driver	Ex	0	3	100	0.008	100	300	85.01 ± 2.86	1.18	28.34 ± 3.94
Hypoxia effect	I-Aug	Ex	0	3	100	0.012	100	300	84.94 ± 3.00	1.18	28.31 ± 4.40
Hypoxia effect	I-Dec	Ex	0	3	100	0.025	100	300	84.94 ± 3.00	1.18	28.31 ± 4.40
Hypoxia effect	E-Aug-BS	Ex	0	3	100	0.0	100	300	84.94 ± 3.00	1.18	28.31 ± 4.40
Hypoxia effect	I-Aug-BS/PHR	Ex	0	3	100	0.0	100	300	84.94 ± 3.00	1.18	28.31 ± 4.40
Hypoxia effect	E-Dec-P	Ex	0	2	100	0.013	100	300	84.94 ± 3.00	1.18	28.31 ± 4.40
Hypoxia effect	E-Dec-T	Ex	0	3	100	0.0	100	300	84.94 ± 3.00	1.18	28.31 ± 4.40
Hypoxia effect	E-Aug-late-HT	Ex	0	3	100	0.0	100	300	84.94 ± 3.00	1.18	28.31 ± 4.40
Hypoxia effect	E-Aug-late	Ex	0	3	100	0.013	100	300	84.94 ± 3.00	1.18	28.31 ± 4.40
Hypoxia effect	E-Aug-early	Ex	0	3	100	0.01	100	300	84.94 ± 3.00	1.18	28.31 ± 4.40

ACKNOWLEDGMENTS

We thank P. Barnhill, K. Ruff, K. Ross, and C. Strohmenger for excellent technical assistance and Drs. Christopher G. Wilson and A. H. Hutchison for helpful discussions.

GRANTS

This work was supported by National Institute of Neurological Disorders and Stroke Grants R01 NS-046062 as part of the NSF/NIH Collaborative Research in Computational Neuroscience (CRCNS) Program, R37 NS-019814, and R01 NS-057815 to I. A. Rybak and N. A. Shevtsova.

REFERENCES

Alheid GF, Gray PA, Jiang MC, Feldman JL, McCrimmon DR. Parvalbumin in respiratory neurons of the ventrolateral medulla of the adult rat. *J Neurocytol* 31: 693–717, 2002.

Alheid GF, Milsomb WK, McCrimmon DR. Pontine influences on breathing: an overview. *Respir Physiol Neurobiol* 143: 105–114, 2004.

Anders K, Ballantyne D, Bischoff AM, Lalley PM, Richter DW. Inhibition of caudal medullary expiratory neurons by retrofacial inspiratory neurons in the cat. *J Physiol* 437: 1–25, 1991.

Arata A, Hernandez YM, Lindsey BG, Morris KF, Shannon R. Transient configurations of baroresponsive respiratory-related brain stem neuronal assemblies in the cat. *J Physiol* 525: 509–530, 2000.

Baekey DM, Morris KF, Gestreau C, Li Z, Lindsey BG, Shannon R. Medullary respiratory neurones controlling laryngeal motoneurone discharge during eupnoea and fictive cough in the cat. *J Physiol* 534: 565–581, 2001.

Baekey DM, Morris KF, Nuding SC, Segers LS, Lindsey BG, Shannon R. Medullary raphe neuron activity is altered during fictive cough in the decerebrate cat. *J Appl Physiol* 94: 93–100, 2003.

Baekey DM, Morris KF, Nuding SC, Segers LS, Lindsey BG, Shannon R. Involvement of ventral respiratory group neurons in the fictive expiration reflex. *J Appl Physiol* 96: 2057–2072, 2004.

Balis UJ, Morris KF, Koleski J, Lindsey BG. Simulations of a ventrolateral medullary neural network for respiratory rhythmogenesis inferred from spike train cross-correlation. *Biol Cybern* 70: 311–327, 1994.

Batsel HL. Some functional properties of bulbar respiratory units. *Exp Neurol* 11: 341–366, 1965.

Bianchi AL, Denavit-Saubie M, Champagnat J. Central control of breathing in mammals: neuronal circuitry, membrane properties, and neurotransmitters. *Physiol Rev* 75: 1–45, 1995.

Bolser DC, Poliacek I, Jakus J, Fuller DD, Davenport PW. Neurogenesis of cough, other airway defensive behaviors and breathing: a holarchical system? *Respir Physiol Neurobiol* 152: 255–265, 2006.

Bonham AC, McCrimmon DR. Neurons in a discrete region of the nucleus tractus solitarius are required for the Breuer-Hering reflex in the rat. *J Physiol* 427: 261–280, 1990.

Breen BJ, Gerken WC, Butera RJ Jr. Hybrid integrate-and-fire model of a bursting neuron. *Neural Comput* 15: 2843–2862, 2003.

Butera RJ, Rinzel JR, Smith JC. Models of respiratory rhythm generation in the pre-Bötzinger complex. I. Bursting pacemaker neurons. *J Neurophysiol* 82: 382–397, 1999.

Clark FJ, von Euler C. On the regulation of depth and rate of breathing. *J Physiol* 222: 267–295, 1972.

Cohen MI. Neurogenesis of respiratory rhythm in the mammal. *Physiol Rev* 59: 1105–1173, 1979.

Cohen MI, Huang W-X, Barnhardt R, See WR. Timing of medullary late-inspiratory neuron discharges: vagal afferent effects indicate possible off-switch function. *J Neurophysiol* 69: 1784–1787, 1993.

Cohen MI, Shaw CF. Role in the inspiratory off-switch of vagal inputs to rostral pontine inspiratory-modulated neurons. *Respir Physiol Neurobiol* 143: 127–140, 2004.

Del Negro CA, Koshiya N, Butera RJ, Smith JC. Persistent sodium current, membrane properties, and intrinsic bursting behavior of pre-Bötzinger complex inspiratory neurons in vitro. *J Neurophysiol* 88: 2242–2250, 2002.

Dick TE, Bellingham MC, Richter DW. Pontine respiratory neurons in anesthetized cats. *Brain Res* 636: 259–269, 1994.

Dick TE, Morris KF, Baekey DM, Nuding SC, Segers LS, Lindsey BG, Shannon R. Dorsolateral pontine respiratory modulated activity before and after vagotomy in decerebrate cats. *Soc Neurosci Abstr* 171.1, 2002.

Dick TE, Shannon R, Lindsey BG, Nuding SC, Segers LS, Baekey DM, Morris KF. Pontine respiratory-modulated activity before and after vagotomy in decerebrate cats. *J Physiol* doi:10.1113/jphysiol.2008.152108.

Douglas CL, Demarco GJ, Baghdoyan HA, Lydic R. Pontine and basal forebrain cholinergic interaction: implications for sleep and breathing. *Respir Physiol Neurobiol* 143: 251–262, 2004.

Duffin J. A model of respiratory rhythm generation. *Neuroreport* 2: 623–626, 1991.

Duffin J. Functional organization of respiratory neurones: a brief review of current questions and speculations. *Exp Physiol* 89: 517–529, 2004.

Duffin JA, Ezure K, Lipski J. Breathing rhythm generation: focus on the rostral ventrolateral medulla. *News Physiol Sci* 10: 133–140, 1995.

Dunin-Barkowski WL, Dick TE, Orem JM, Rybak IA, Morris KF, O'Connor R, Lindsey BG. L-plotting of multidimensional data: applications for the respiratory pattern analysis. *Soc Neurosci Abstr* 154.9, 2006.

Dunin-Barkowski WL, Escobar AL, Lovering AT, Orem JM. Respiratory pattern generator model using Ca^{2+}-induced Ca^{2+} release in neurons shows both pacemaker and reciprocal network properties. *Biol Cybern* 89: 274–288, 2003.

Eisenberg MS. Incidence and significance of gasping or agonal respirations in cardiac arrest patients. *Curr Opinion Crit Care* 12: 204–206, 2006.

Elsen FP, Ramirez J. Calcium currents of rhythmic neurons recorded in the isolated respiratory network of neonatal mice. *J Neurosci* 18: 10652–10662, 1998.

England SJ, Melton JE, Douse MA, Duffin J. Activity of respiratory neurons during hypoxia in the chemodenervated cat. *J Appl Physiol* 78: 856–861, 1995.

Ezure K. Synaptic connections between medullary respiratory neurons and considerations on the genesis of respiratory rhythm. *Prog Neurobiol* 35: 429–450, 1990.

Ezure K. Respiration-related afferents to parabrachial pontine regions. *Respir Physiol Neurobiol* 143: 167–175, 2004.

Ezure K, Manabe M, Otake K. Excitation and inhibition of medullary inspiratory neurons by two types of burst inspiratory neurons in the cat. *Neurosci Lett* 104: 303–308, 1989.

Ezure K, Otake K, Lipski J, She RB. Efferent projections of pulmonary rapidly adapting receptor relay neurons in the cat. *Brain Res* 564: 268–278, 1991.

Ezure K, Tanaka I. GABA, in some cases together with glycine, is used as the inhibitory transmitter by pump cells in the Hering-Breuer reflex pathway of the rat. *Neurosci* 127: 409–417, 2004.

Ezure K, Tanaka I. Distribution and medullary projection of respiratory neurons in the dorsolateral pons of the rat. *Neurosci* 14: 1011–1023, 2006.

Feldman JL. Neurophysiology of breathing in mammals. In: *Handbook of Physiology. The Nervous System. Intrinsic Regulatory Systems of the Brain.* Bethesda, MD: Am. Physiol. Soc., 1986, sect. 1, vol. IV, p. 463–524.

Felder RB, Mifflin SW. Modulation of carotid sinus afferent input to nucleus tractus solitarius by parabrachial stimulation. *Circ Res* 63: 35–49, 1988.

Feldman JL, Cohen MI, Wolotsky P. Powerful inhibition of pontine respiratory neurons by pulmonary afferent activity. *Brain Res* 104: 341–346, 1976.

Feldman JL, Del Negro CA. Looking for inspiration: new perspectives on respiratory rhythm. *Nat Rev Neurosci* 7: 232–242, 2006.

Feldman JL, Mitchell GS, Nattie EE. Breathing: Rhythmicity, plasticity, chemosensitivity. *Annu Rev Neurosci* 26: 239–266, 2003.

Feldman JL, Speck DF. Interactions among inspiratory neurons in dorsal and ventral respiratory groups in cat medulla. *J Neurophysiol* 49: 472–490, 1983.

Fortuna MG, West GH, Stornetta RL, Guyenet PG. Bötzinger expiratory-augmenting neurons and the parafacial respiratory group. *J Neurosci* 28: 2506–2515, 2008.

Fung ML, St-John WM. The functional expression of a pontine pneumotaxic center in neonatal rats. *J Physiol* 489: 579–591, 1995.

Gaytán SP, Calero F, Núñez-Abades PA, Morillo AM, Pasaro R. Pontomedullary efferent projections of the ventral respiratory neuronal subsets of the rat. *Brain Res Bull* 42: 323–334, 1997.

Gottschalk A, Ogilvie MD, Richter DW, Pack AI. Computational aspects of the respiratory pattern generator. *Neural Comput* 6: 56–68, 1994.

Gray PA, Janczewski WA, Mellen N, McCrimmon DR, Feldman JL. Normal breathing requires pre-Bötzinger complex neurokinin-1 receptor-expressing neurons. *Nat Neurosci* 4: 927–930, 2001.

Haji A, Okazaki M, Yamazaki H, Takeda R. Physiological properties of late inspiratory neurons and their possible involvement in inspiratory off-switching in cats. *J Neurophysiol* 87: 1057–1067, 2002.

Hamilton RB, Ellenberger H, Liskowsky D, Schneiderman N. Parabrachial area as mediator of bradycardia in rabbits. *J Autonom Nerv Sys* 4: 261–281, 1981.

Harper RM, Kinney HC, Fleming PJ, Thach BT. Sleep influences on homeostatic functions: implications for sudden infant death syndrome *Respir Physiol* 119: 123–132, 2000.

Hsieh YH, Siegel RE, Dick TE. Pontine GABAergic pathways: role and plasticity in the hypoxic ventilatory response. *Respir Physiol Neurobiol* 143: 141–153, 2004.

Jiang C, Lipski J. Extensive monosynaptic inhibition of ventral respiratory group neurons by augmenting neurons in the Bötzinger complex in the cat. *Exp Brain Res* 81: 639–648, 1990.

Kirsten EB, St-John WM. A feline decerebration technique with low mortality and long-term homeostasis. *J Pharmacol Methods* 1: 263–268, 1978.

Kubin L, Alheid GF, Zuperku EJ, McCrimmon DR. Central pathways of pulmonary and lower airway vagal afferents. *J Appl Physiol* 101: 618–627, 2006.

Kubin L, Fenik V. Pontine cholinergic mechanisms and their impact on respiratory regulation. *Respir Physiol Neurobiol* 143: 235–249, 2004.

Lara JP, Parkes MJ, Silva-Carvhalo L, Izzo P, Dawid-Milner MS, Spyer KM. Cardiovascular and respiratory effects of stimulation of cell bodies of the parabrachial nuclei in the anaesthetized rat. *J Physiol* 477: 321–329, 1994.

Li Z, Morris KF, Baekey DM, Shannon R, Lindsey BG. Multimodal medullary neurons and correlational linkages of the respiratory network. *J Neurophysiol* 82: 188–201, 1999.

Lindsey BG, Arata A, Morris KF, Hernandez YM, Shannon R. Medullary raphe neurones and baroreceptor modulation of the respiratory motor pattern in the cat. *J Physiol* 512: 863–882, 1998.

Lindsey BG, Morris KF, Segers LS, Shannon R. Respiratory neuronal assemblies. *Respir Physiol* 122: 183–196, 2000.

Lindsey BG, O'Connor R, Nuding SC, Segers LS, Morris KF, Shannon R, Rybak IA. A consolidated hybrid pontine-medullary respiratory network model: Simulated predictions and experimental testing. *Soc Neurosci Abstr* 866.7, 2005.

Lindsey BG, Ross A, O'Connor R, Morris KF, Nuding SC, Segers LS, Shannon R, Dick TE, Dunin-Barkowski WL, Orem JM, Solomon IC, Rybak IA. Modulation and reconfiguration of the pontomedullary respiratory network: a computational modeling study (Abstract). *FASEB J* 610.11, 2007.

Lindsey BG, Segers LS, Morris KF, Hernandez YM, Saporta S, Shannon R. Distributed actions and dynamic associations in respiratory-related neuronal assemblies of the ventrolateral medulla and brainstem midline: evidence from spike train analysis. *J Neurophysiol* 72: 1830–1851, 1994.

Lindsey BG, Segers LS, Shannon R. Discharge patterns of augmenting expiratory neurons in rostral lateral medulla of cat: regulation by concurrent network processes. *J Neurophysiol* 61: 1185–1196, 1989a.

Lindsey BG, Segers LS, Shannon R. Functional associations among simultaneously monitored lateral medullary respiratory neurons in the cat. II. Evidence for inhibitory actions of expiratory neurons. *J Neurophysiol* 57: 1101–1117, 1987.

Lindsey BG, Shannon R, Gerstein GL. Gravitational representation of simultaneously recorded brain stem respiratory neuron spike trains. *Brain Res* 483: 373–378, 1989b.

Lovering AT, Dunin-Barkowski WL, Vidruk EH, Orem JM. Ventilatory response of the cat to hypoxia in sleep and wakefulness. *J Appl Physiol* 95: 545–554, 2003.

Lovering AT, Fraigne JJ, Dunin-Barkowski WL, Vidruk EH, Orem JM. Medullary respiratory neural activity during hypoxia in NREM and REM sleep in the cat. *J Neurophysiol* 95: 803–810, 2006.

Lumsden T. Observations on the respiratory centres in the cat. *J Physiol* 57: 153–160, 1923.

MacGregor RJ. *Neural and Brain Modeling*. New York: Academic, 1987.

Marckwald M. Die athembewegunge und dere innervation beim kaninchen. *Ztschr Biol* 23: 149–283, 1887.

Millhorn DE. Stimulation of raphe (obscurus) nucleus causes long-term potentiation of phrenic nerve activity in cat. *J Physiol* 381: 169–179, 1986.

Mitchell GS, Johnson SM. Neuroplasticity in respiratory motor control. *J Appl Physiol* 94: 358–374, 2003.

Morris KF, Arata A, Shannon R, Lindsey BG. Inspiratory drive and phase duration during carotid chemoreceptor stimulation in the cat: medullary neurone correlations. *J Physiol* 491: 241–259, 1996.

Morris KF, Baekey DM, Nuding SC, Dick TE, Shannon R, Lindsey BG. Plasticity in respiratory motor control: invited review: neural network plasticity in respiratory control. *J Appl Physiol* 94: 1242–1252, 2003.

Morris KF, Lindsey BG, Baekey DM, Nuding SC, Segers LS, Shannon R, O'Connor RE, Dick TE. Cardiorespiratory rhythms in spike trains of caudal raphe and pontine neurons in cats: insights from computational models of acute vagotomy. *Soc Neurosci Abstr* 230.11, 2007.

Morris KF, Solomon IC, Nuding SC, Segers LS, Lindsey BG. Distributed processing by multiple brain stem networks during hypoxia-induced gasps and augmented bursts. *Soc Neurosci Abstr* 636.4, 2005.

Morrison SF, Cravo SL, Wilfehrt HM. Pontine lesions produce apneusis in the rat. *Brain Res* 652: 83–86, 1994.

Mulkey D, Stornetta R, Weston M, Simmons J, Parker A, Bayliss D, Guyenet P. Respiratory control by ventral surface chemoreceptor neurons in rats. *Nat Neurosci* 7: 360–1369, 2004.

Neverova NV, Saywell SA, Nashold LJ, Mitchell GS, Feldman JL. Episodic stimulation of alpha1-adrenoreceptors induces protein kinase C-dependent persistent changes in motoneuronal excitability. *J Neurosci* 27: 4435–4442, 2007.

Nuding SC, Lindsey BG, Segers LS, Baekey DM, Dick TE, Shannon R, Morris KF. Pontomedullary respiratory correlational assembly dynamics during transient hyperventilatory apnea (Abstract). *FASEB J* 19: 921.20, 2005.

Nuding SC, Segers LS, Morris KF, Solomon IC, Dick TE, Shannon R, Lindsey BG. Recurrent connections between the pontine respiratory group and ventrolateral medullary respiratory column through parallel functional pathways (Abstract). *FASEB J* 20: 230.7, 2006.

Núñez-Abades PA, Spielmann JM, Barrionuevo G, Cameron WE. In vitro electrophysiology of developing genioglossal motoneurons in the rat. *J Neurophysiol* 70: 1401–1411, 1993.

Ogilvie MD, Gottschalk A, Anders K, Richter DW, Pack AI. A network model of respiratory rhythmogenesis. *Am J Physiol Regulatory Integrative Comp Physiol* 263: R962–R975, 1992.

Okazaki M, Takeda R, Yamazaki H, Haji A. Synaptic mechanisms of inspiratory off-switching evoked by pontine pneumotaxic stimulation in cats. *Neurosci Res* 44: 101–110, 2002.

Onimaru H, Kumagawa Y, Homma I. Respiration-related rhythmic activity in the rostral medulla of newborn rats. *J Neurophysiol* 96: 55–61, 2006.

Orem J, Dick T. Consistency and signal strength of respiratory neuronal activity. *J Neurophysiol* 50: 1098–1107, 1983.

Orer HS, Gebber GL, Barman SM. Medullary lateral tegmental field neurons influence the timing and pattern of phrenic nerve activity in cats *J Appl Physiol* 101: 521–530, 2006.

Pace RW, Mackay DD, Feldman JL, Del Negro CA. Inspiratory bursts in the pre-Bötzinger complex depend on a calcium-activated non-specific cation current linked to glutamate receptors in neonatal mice. *J Physiol* 582: 113–125, 2007a.

Pace RW, Mackay DD, Feldman JL, Del Negro CA. Role of persistent sodium current in mouse pre-Bötzinger Complex neurons and respiratory rhythm generation. *J Physiol* 580: 485–496, 2007b.

Paton JFR, Abdala APL, Koizumi H, Smith JC, St-John WM. Respiratory rhythm generation during gasping depends on persistent sodium current. *Nat Neurosci* 9: 311–313, 2006.

Paton JFR, St-John WM. Counterpoint: medullary pacemaker neurons are essential for gasping, but not eupnea, in mammals *J Appl Physiol* 103: 718–720, 2007.

Pierrefiche O, Haji A, Bischoff AM, Richter DW. Calcium current in respiratory neurons of the cat in vivo. *Pfluegers* 438: 817–826, 1999.

Pierrefiche O, Shevtsova NA, St-John WM, Paton JFR, Rybak IA. Ionic currents and endogenous rhythm generation in the pre-Bötzinger Complex: modeling and *in vitro* studies. *Adv Exp Med Biol* 551: 121–126, 2004.

Potts JT, Rybak IA, Paton JFR. Respiratory rhythm entrainment by somatic afferent stimulation. *J Neurosci* 25: 1965–1978, 2005.

Radulovacki M, Pavlovic S, Saponjic J, Carley DW. Modulation of reflex and sleep related apnea by pedunculopontine tegmental and intertrigeminal neurons. *Respir Physiol Neurobiol* 143: 293–306, 2004.

Ramirez JM, Garcia A. Point: Counterpoint: Medullary pacemaker neurons are essential for both eupnea and gasping in mammals vs. medullary pacemaker neurons are essential for gasping, but not eupnea, in mammals. *J Appl Physiol* 103: 717–718, 2007.

Rekling JC, Shao XM, Feldman JL. Electrical coupling and excitatory synaptic transmission between rhythmogenic respiratory neurons in the pre-Bötzinger complex. *J Neurosci 20: RC* 113: 1–5, 2000.

Richter DW. Neural regulation of respiration: rhythmogenesis and afferent control. In: Gregor R, Windhorst U. (Eds.), *Comprehensive Human Physiology*, Vol. II, Springer-Verlag, Berlin, pp. 2079–2095, 1996.

Richter DW, Ballantyne D, Remmers JE. How is the respiratory rhythm generated? A model. *News Physiol Sci* 1: 109–112, 1986.

Richter DW, Champagnat J, **Jacquin T**, **Benacka R.** Calcium currents and calcium-dependent potassium currents in mammalian medullary respiratory neurons. *J Physiol* 470: 23–33, 1993.

Richter DW, Spyer KM. Studying rhythmogenesis of breathing: comparison of in vivo and in vitro models. *Trends Neurosci* 24: 464–472, 2001.

Rybak IA, Abdala AP, Markin SN, Paton JF, Smith JC. Spatial organization and state-dependent mechanisms for respiratory rhythm and pattern generation. *Prog Brain Res* 165: 201–220, 2007a.

Rybak IA, Büsselberg D, Peña F, Eugenín JL, Muller KJ, Lalley PM, Potts JT. Point-counterpoint comments: medullary pacemaker neurons are essential for both eupnea and gasping in mammals vs. medullary pacemaker neurons are essential for gasping, but not eupnea, in mammals. *J Appl Physiol* 103: 723, 2007b.

Rybak IA, Paton JFR, Rogers RF, St-John WM. Generation of the respiratory rhythm: state-dependency and switching. *Neurocomputing* 44–46: 603–612, 2002.

Rybak IA, Paton JFR, Schwaber JS. Modeling neural mechanisms for genesis of respiratory rhythm and pattern. I. Models of respiratory neurons. *J Neurophysiol* 77: 1994–2006, 1997a.

Rybak IA, Paton JFR, Schwaber JS. Modeling neural mechanisms for genesis of respiratory rhythm and pattern. II. Network models of the central respiratory pattern generator. *J Neurophysiol* 77: 2007–2026, 1997b.

Rybak IA, Ptak K, Shevtsova NA, McCrimmon DR. Sodium currents in neurons from the rostroventrolateral medulla of the rat. *J Neurophysiol* 90: 1635–1642, 2003a.

Rybak IA, Shevtsova NA, Paton JFR, Dick TE, St-John WM, Mörschel M, Dutschmann M. Modeling the ponto-medullary respiratory network. *Respir Physiol Neurobiol* 143: 307–319, 2004a.

Rybak IA, Shevtsova NA, Ptak K, McCrimmon DR. Intrinsic bursting activity in the pre-Bötzinger complex: role of persistent sodium and potassium currents. *Biol Cybern* 90: 59–74, 2004b.

Rybak IA, Shevtsova NA, St-John WM, Paton JFR, Pierrefiche O. Endogenous rhythm generation in the pre-Bötzinger complex and ionic currents: modeling and in vitro studies. *Eur J Neurosci* 18: 239–257, 2003b.

Sant'Ambrogio G, Widdicombe J. Reflexes from airway rapidly adapting receptors. *Respir Physiol* 125: 33–44, 2001.

Sears TA, Berger AJ, **Phillipson EA.** Reciprocal tonic activation of inspiratory and expiratory motoneurones by chemical drives. *Nature* 299: 728–730, 1982.

Segers LS, Nuding SC, Dick TE, Shannon R, Baekey DM, Solomon IC, Morris KF, Lindsey BG. Functional connectivity in the pontomedullary respiratory network. *J Neurophysiol* doi:10.1152/jn.90414.2008.

Segers LS, Shannon R, Lindsey BG. Interactions between rostral pontine and ventral medullary respiratory neurons. *J Neurophysiol* 54: 318–334, 1985.

Segers LS, Shannon R, Saporta S, Lindsey BG. Functional associations among simultaneously monitored lateral medullary respiratory neurons in the cat. I. Evidence for excitatory and inhibitory actions of inspiratory neurons. *J Neurophysiol* 57: 1078–1100, 1987.

Shannon R, Baekey DM, Morris KF, Li Z, Lindsey BG. Functional connectivity among ventrolateral medullary respiratory neurones and responses during fictive cough in the cat. *J Physiol* 525: 207–224, 2000.

Shannon R, Baekey DM, Morris KF, Lindsey BG. Ventrolateral medullary respiratory network and a model of cough motor pattern generation. *J Appl Physiol* 84: 2020–2035, 1998.

Shannon R, Baekey DM, Morris KF, Nuding SC, Segers LS, Lindsey BG. Pontine respiratory group neuron discharge is altered during fictive cough in the decerebrate cat. *Respir Physiol Neurobiol* 142: 43–54, 2004a.

Shannon R, Baekey DM, Morris KF, Nuding SC, Segers LS, Lindsey BG. Production of reflex cough by brain stem respiratory networks. *Pul Pharm Ther* 17: 369–376, 2004b.

Shannon R, Ross AJ, O'Connor RE, Morris KF, Rybak IA, Lindsey BG. Simulations of the cough reflex: Reconfiguration of a hybrid pontine-medullary respiratory network model. In: *Oxford Conference (X) on Modeling and Control of Breathing. Integration in Respiratory Control: From Genes to Systems*. Lake Louise, Alberta, Canada, 2006.

Smith JC, Abdala AP, Koizumi H, Rybak IA, Paton JFR. Spatial and functional architecture of the Mammalian brain stem respiratory network: a hierarchy of three oscillatory mechanisms. *J Neurophysiol* 98: 3370–3387, 2007.

Smith JC, Butera RJ, Koshiya N, Del Negro C, Wilson CG, Johnson SM. Respiratory rhythm generation in neonatal and adult mammals: the hybrid pacemaker-network model. *Respir Physiol Neurobiol* 122: 131–147, 2000.

Smith JC, Ellenberger HH, Ballanyi K, Richter DW, Feldman JL. Pre-Bötzinger complex: a brain stem region that may generate respiratory rhythm in mammals. *Science* 254: 726–729, 1991.

Solomon IC. Excitation of phrenic and sympathetic output during acute hypoxia: contribution of medullary oxygen detectors. *Respir Physiol* 121: 101–117, 2000.

Solomon IC. Modulation of gasp frequency by activation of pre-Bötzinger complex in vivo. *J Neurophysiol* 87: 1664–1668, 2002.

Solomon IC. Influence of respiratory network drive on phrenic motor output evoked by activation of cat pre-Bötzinger complex. *Am J Physiol Regulatory Integrative Comp Physiol* 284: R455–R466, 2003.

Song G, Poon CS. Functional and structural models of pontine modulation of mechanoreceptor and chemoreceptor reflexes. *Respir Physiol Neurobiol* 143: 281–292, 2004.

St-Jacques R, St-John WM. Transient, reversible apnoea following ablation of the pre-Bötzinger complex in rats. *J Physiol* 520: 303–314, 1999.

St-John WM. Neurogenesis of patterns of automatic ventilatory activity. *Prog Neurobiol* 56: 97–117, 1998.

St-John WM, Paton JFR. Defining eupnea. *Respir Physiol Neurobiol* 139: 97–103, 2003a.

St-John WM, Paton JFR. Respiratory-modulated neuronal activities of the rostral medulla which may generate gasping. *Respir Physiol Neurobiol* 135: 97–101, 2003b.

St-John WM, Rybak IA, Paton JFR. Potential switch from eupnea to fictive gasping after blockade of glycine transmission and potassium channels. *Am J Physiol Regulatory Integrative Comp Physiol* 283: R721–R731, 2002.

Thuot F, Lemaire D, Dorion D, Letourneau, Praud JP. Active glottal closure during anoxic gasping in lambs. *Respir Physiol* 128: 205–218, 2001.

von Euler C. Brain stem mechanism for generation and control of breathing pattern. In: *Handbook of Physiology. The Respiratory System. Control of Breathing.* Washington, DC: Am. Physiol. Soc.,1986, sect. 3, vol. II, p. 1–67.

Wang W, Fung ML, St-John WM. Pontile regulation of ventilatory activity in the adult rat. *J Appl Physiol* 74: 2801–2811, 1993.